A ONE-DIMENSIONAL MIXED LAYER OCEAN AND SEA ICE MODEL WITH PRESCRIBED OCEANIC HEAT TRANSPORT

by T. G. Jensen, D. A. Dazlich, and D. A. Randall

Colorado State University

DEPARTMENT OF ATMOSPHERIC SCIENCE

PAPER NO. 593

A ONE-DIMENSIONAL MIXED LAYER OCEAN AND SEA ICE MODEL WITH PRESCRIBED OCEANIC HEAT TRANSPORT

by

Tommy G. Jensen, Donald A. Dazlich and David A. Randall

Research supported by the
U.S. Department of Energy
under Grant number DE-FG02-89ER69027

Department of Atmospheric Science
Colorado State University
Fort Collins, CO

December 1995

Atmospheric Science Paper No. 593

A ONE-DIMENSIONAL MIXED LAYER OCEAN AND SEA ICE MODEL WITH PRESCRIBED OCEANIC HEAT TRANSPORT

Tommy G. Jensen, Donald A. Dazlich and David A. Randall

Dept. of Atmospheric Science
Colorado State University
Fort Collins, Colorado

Abstract

We describe a simple two-layer thermodynamic ocean-ice model, which has been developed for coupling to an atmospheric general circulation model (GCM). The model ocean is thermally active above the annual mixed layer maximum. It consists of an upper mixed layer, which exchanges heat with the atmosphere through radiative, latent and sensible heat fluxes, and a deeper oceanic layer, which exchanges heat with the mixed layer through entrainment and detrainment. Heat transport caused by advection and diffusion is calculated as the implied oceanic heat divergence/convergence resulting from net heat flux into the ocean when the GCM is forced by observed sea surface temperature (SST). The variation in mixed layer depth is prescribed from climatology, while the SST and heat storage between the mixed layer depth and its annual maximum is predicted by the model. Cooling of sea water at its freezing point results in formation of sea ice and possible accumulation of snow. Ice and snow thickness are prognostic variables in the thermodynamic sea ice model.

Results are presented from two 30 year runs with oceanic mixed layer and sea ice model coupled to the CSU GCM. One run demonstrates the ability of the coupled system to simulate the current climate while the second coupled run is an instantaneous $2 \times CO_2$ scenario.

1. INTRODUCTION

The ocean plays an important role in the Earth's climate is important and must be included in climate models. The ocean has in early studies been represented by prescribed sea surface temperatures (SST). Ocean models range from swamp layers, which supply moisture to the atmosphere, but cannot store heat (see for instance Washington and Meehl, 1983), to full general circulation models of the ocean (Bryan et al.,1975; Manabe et al., 1975; Washington et al., 1980). In between fall simple oceanic mixed layer models such as those used by Manabe and Stouffer, (1980), Washington and Meehl,(1984) and Hansen et al., (1984). The ocean model presented here falls in this last category.

When the mixed-layer temperature reaches the freezing point for seawater (about 271°K), sea ice forms. Further cooling should lead to thicker sea ice. The zero-layer formulation by Semtner (1976) provides a simple one-dimensional thermodynamic sea ice model, and was previously used by Washington and Meehl (1984), who assumed that the heat flux from the mixed layer to the sea ice is zero. When sea ice is present, the ocean temperature in their model remains at the freezing point. A one-dimensional thermodynamic very similar to that of Semtner (1976) is implemented in our model ocean. Jensen et al., (1991) presented some aspects of an early version of this combined ocean and sea ice model. In this report a very detailed description is given.

1.1 Mixed Layer Models

The simplest active representation of the ocean is a layer of constant depth, which can store heat determined from exchange with the atmosphere. A mixed layer of constant depth h_0 has a temperature given by

$$\rho_w c_w \frac{\partial T}{\partial t} = \frac{F}{h_0} \tag{1}$$

where ρ_w is the average density of the mixed layer, c_w is the heat capacity of seawater and F is the net heat flux into the ocean. Unless the heat flux F integrated over a long period vanishes, a local warming or cooling trend will occur, resulting in locally higher or lower sea surface temperatures. Feedback from the ocean to the atmosphere is through changes in long wave radiation, latent and sensible heat flux, which eventually will regulate the SST towards a steady state. This type of mixed layer model was used by Washington and Meehl, (1984) to study climate sensitivity to a doubling of CO_2 in the atmosphere. They used a uniform depth of 50 m for the mixed layer.

One problem is that internal heat transport in the ocean is very large, e.g. the advection of heat by western boundary currents such as the Gulf Stream. Without oceanic heat transport, local SST cannot be predicted correctly by a mixed layer model.

A simple way to compute the oceanic heat transport from an atmospheric GCM has been described by Miller et al. (1983) and Russell et al. (1985). An implicitly obtained convergence or divergence of heat in the ocean can be used as additional forcing of a simple mixed layer ocean similar to the one described above. Hansen et al. (1984; 1988) used a mixed layer model with such a prescribed heat transport, also referred to as a Q-flux model. A similar ocean model is described below and has been coupled to the CSU GCM.

2. CSU SLAB OCEAN AND SEA ICE MODELS

Earlier versions of the CSU GCM used prescribed SST and sea ice distributions. However, climatological SST, which represents an infinite oceanic heat capacity, does not allow a realistic response to changes in atmospheric forcing, such as those caused by increased concentrations of CO_2.

The model ocean consists of a thermodynamically active mixed layer with prescribed seasonal heat transports and mixed layer depths. The sea surface temperature is predicted. The approach is similar to that used in the Goddard Institute for Space Studies (GISS) model (Hansen et al., 1984). Our sea ice model is a modified, implicit one-layer version of the Semtner (1976) model, with snow depth, ice thickness and ice temperature as prognostic variables. The model formulations are described in detail below.

2.1 Oceanic Heat Transport

We compute the implied heat transport in the ocean using the method described by Miller et al. (1983) and Russell et al. (1985).

The net heat flux F *into* the ocean can be denoted as follows:

$$F = (1 - \alpha_s)S^{\downarrow} + F^{\downarrow} - F^{\uparrow} + H + LE \equiv S_R + S_O \qquad (2)$$

where $S^{\downarrow}$ is the downward solar radiation, α_s is the surface albedo, $F\downarrow$ ($F\uparrow$) is the downward (upward) thermal radiation, H is the (downward) sensible heat flux and LE is the (downward) latent heat flux from evaporation.

The heat flux F can be found from a run with a GCM, where the seasonal variation of the sea surface temperature is prescribed by monthly observations. (Russell et al., 1985) suggest that a time filter should be applied to isolate the annual and semi-annual periods if F is based on a short GCM simulation. A complex Fourier transform which can be used for filtering is given the Appendix.

The heat content E_u in the upper ocean can be calculated from observations as

$$E_u = \rho_w c_w \int_{-h_{max}}^{0} T(z)dz + \rho_i h_i(-L + c_i(T_i - T_o) - c_w(T(0) - T_o)) \qquad (3)$$

where the upper ocean is defined as the water column above the annual maximum depth, h_{max}, of the mixed layer (Figure 1). In (3) $T(z)$ is the temperature profile, h_i is the sea ice thickness, L is the latent heat of melting, T_o is the freezing point for sea water and T_i is the sea ice temperature. The densities and specific heat capacities for sea water and sea ice are ρ_w, c_w and ρ_i, c_i respectively. For consistency with the sea ice model, the SST should equal the freezing point whenever sea ice is present.

From observations of NODC expandable bathythermograph (XBT) data Russell et al. (1985), define the depth of the mixed layer as the depth where the ocean temperature has decreased 0.5°C below the SST, with a maximum limit on the mixed depth of 250 m. The data (shown in Fig. 2) was calculated as monthly averages and spatially smoothed.

The mixed layer is assumed to have the temperature of the sea surface. By limiting the maximum mixed layer depth, the e-folding time towards a new planetary equilibrium temperature can be made shorter. Following the calculations of Hansen et al. (1984), this time scale is 8.4 years for a 250 m mixed layer. Our globally averaged mixed layer depth is 132 m, which implies a response time of 4.4 years.

Climatological sea ice thickness observations, which cover the polar areas do not exist. For this reason sea ice thickness have to be calculated from observations of sea ice area coverage. Ice data for the Southern Hemisphere can for instance be obtained from Alexander and Mobley (1974) and for the

Maximum Mixed Layer Depth

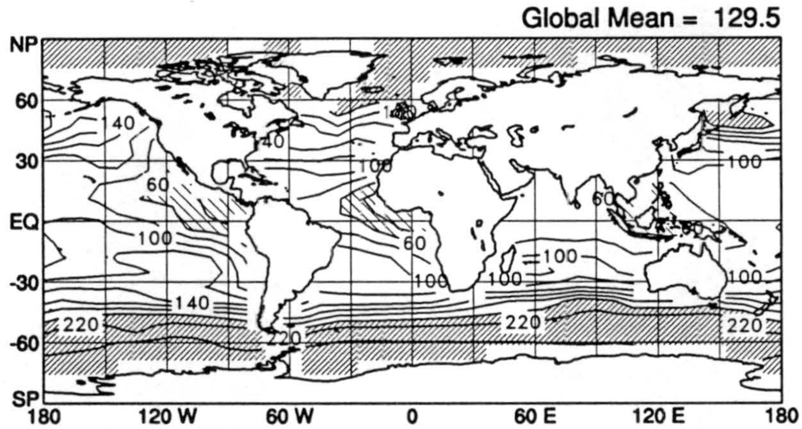

Figure 1: Maximum mixed layer depth based on data from the National Oceanographic Data Center (NODC). The mixed layer is defined as the depth where the temperature is decreased by 0.5°K from the surface value. Mixed layer depths larger than 250 m are truncated. Units are meters.

Northern Hemisphere from Walsh and Johnson (1979).

Formulae which may be applied to calculate sea ice thickness from ice coverage are given here. For areas with some ice throughout the year we use

$$h_i = h_{i1} A_i^2 \tag{4}$$

where A_i is the ice concentration and the maximal sea ice thickness is h_{i1} (2 m in Arctic regions and 1 m in the Antarctic Ocean). For areas which are ice free during part of the year, the sea ice thickness depends on the number of months N with some ice. We use

$$h_i = h_{i2} A_i^2 \sqrt{N} \tag{5}$$

and $h_{i2} = 1$ m for both hemispheres, so a maximum of one meter of annual ice accumulation is assumed in these areas. This formulation is similar to those used by Hansen et al. (1983) and Russell et al. (1985).

The calculation of E_u is started when the mixed layer depth h equals its maximum value h_{max}. During detrainment, when the mixed layer gets shallower, energy is transferred to the heat reservoir below the mixed layer. During entrainment when the mixed layer deepens, water is added from below to form a new mixed layer depth. The temperature of the entrained water is

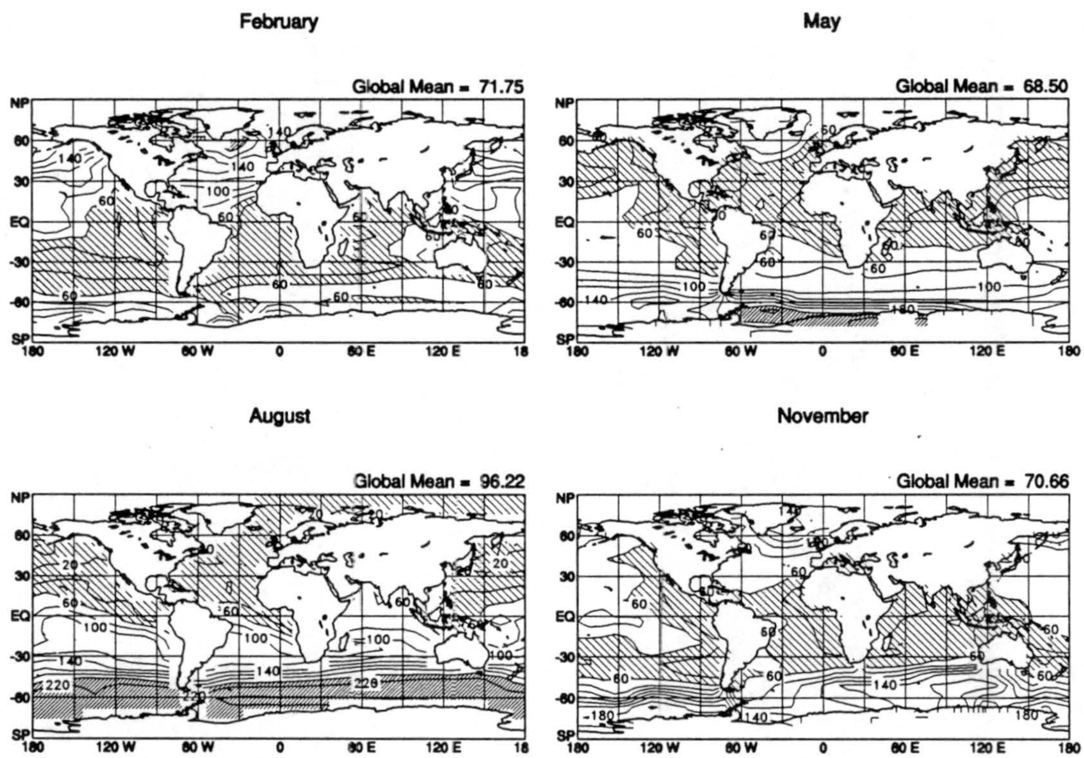

Figure 2: Mixed layer depth for February, May, August and November based on the same data as in Fig. 1. Units are meters.

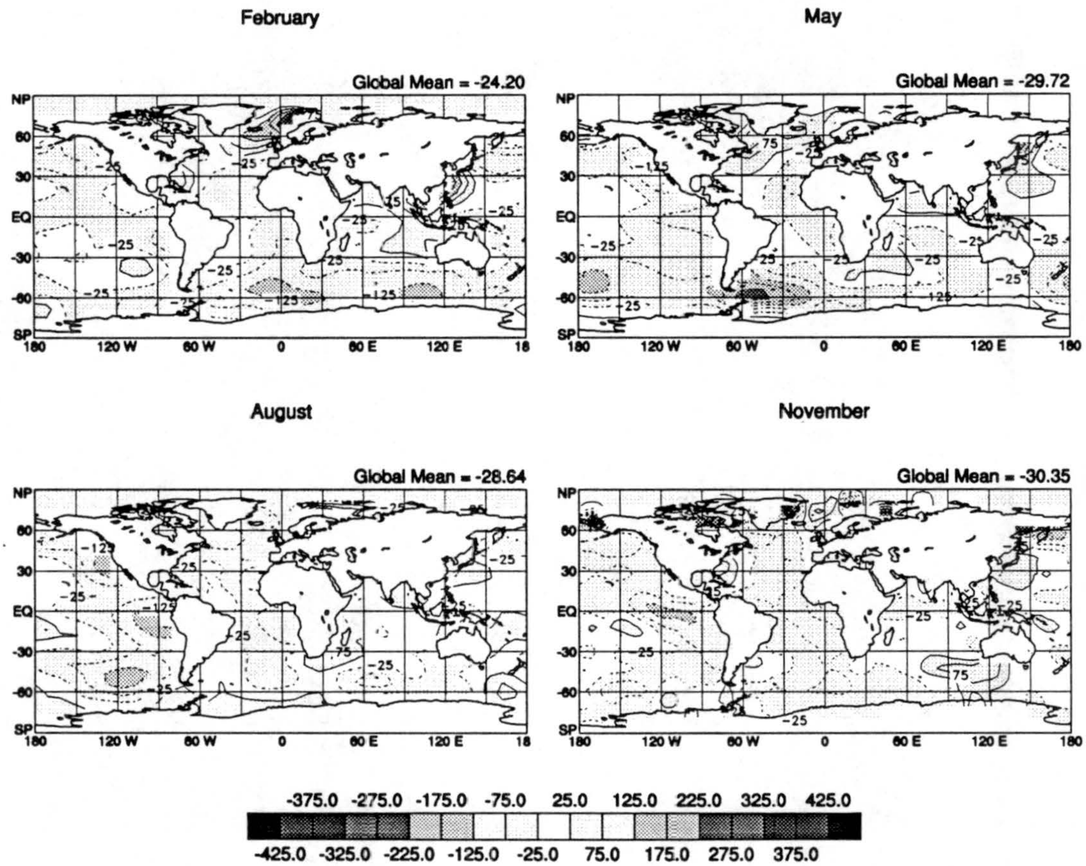

Figure 3: Monthly mean of the oceanic divergence Q. Units are $\mathrm{W/m^2}$.

assumed to be the average of the second layer temperature, consistent with the 2-layer model described below.

Any apparent imbalance in the heat budget of the upper ocean is assumed to be due to an oceanic heat transport Q, *e.g.*

$$Q = \frac{\partial E_u}{\partial t} - F \tag{6}$$

which is calculated from the control run. Figure 3 shows monthly averaged oceanic heat convergence/divergence Q for four months.

2.2 Horizontal and Vertical Heat Transport

For the mixed layer model we do not need to distinguish between vertical and horizontal oceanic heat transports. However, for comparison to data it can be useful to attempt a separation.

The annual (overbar) and spatial (brackets) average of the heat flux is

$$[\overline{F}] = F_o. \tag{7}$$

This represents a net heating or cooling term for the ocean. Russell et al. (1985) found $F_o = 4.0\mathrm{W/m^2}$, and corrected the net downward solar radiation by a factor of $\chi = .9776$ to assure that no net heating of the ocean takes place, *i.e.*, replacing F by

$$F' = \chi \cdot S_R + S_O, \tag{8}$$

which in general implies

$$\chi = \left(1 - F_o/[\overline{S_R}]\right). \tag{9}$$

Another possibility is simply to reduce F to $F' = F - F_o$ everywhere. It is clear from (6) that we must have

$$[\overline{Q}] = Q_o = -F_o. \tag{10}$$

This constant flux imbalance can be thought of as a uniform global flux correction, which is needed for coupled simulations. We have chosen to include it as an additional oceanic heat source. In the present study a value of $F_o = 27.2\mathrm{W/m^2}$ was found from our control model run.

We can split up the oceanic heat transport Q up as

$$Q = Q_H + Q_o - \frac{\partial E_d}{\partial t}, \tag{11}$$

where Q_H is the horizontal heat transport and E_d is the heat storage in the deep ocean.

By forming a spatial average over the globe, the horizontal oceanic heat transport Q_H vanishes, so from (6) and (11)

$$[F'] = \frac{\partial [E_u]}{\partial t} + \frac{\partial [E_d]}{\partial t}. \tag{12}$$

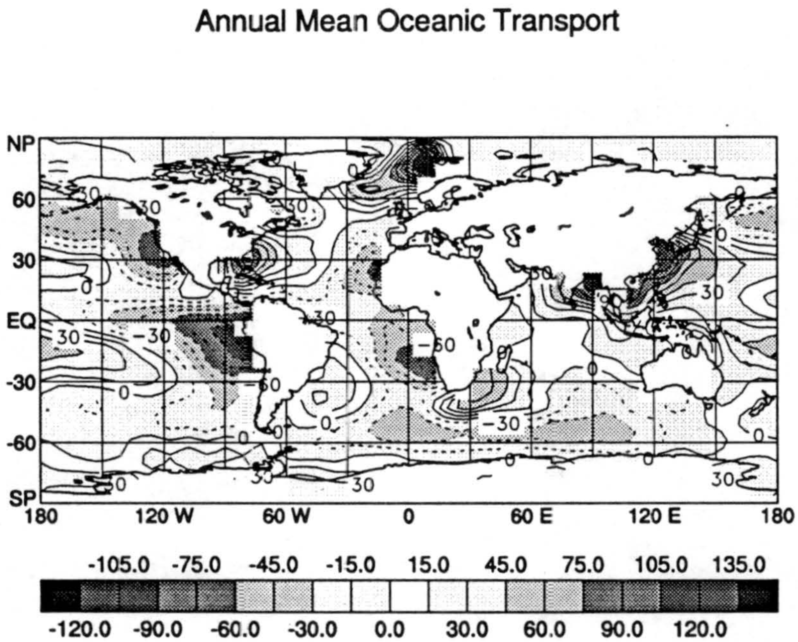

Figure 4: Annual mean of the horizontal oceanic heat transport. Units are W/m^2.

The first two quantities are known, so the temporal variation of the global average of the deep sea heat content is easily calculated. Differentiation may be performed by the Fourier spectral collocation method for accuracy, (see Appendix). By the additional assumption that the temporal variation in deep ocean heat content is spatially uniform, we are able to estimate the horizontal oceanic heat convergence or divergence as

$$Q_H = \frac{\partial E_u}{\partial t} + \frac{\partial [E_d]}{\partial t} - F - Q_o \tag{13}$$

Figure 4 shows the annual average of the horizontal oceanic heat divergence, Q_H. Rather detailed features of the ocean general circulation such as warm western boundary currents, e.g. the Gulf Stream, the Kuroshio and the Algulhas Currents, and upwelling along the west coasts of the continents and the equatorial East Pacific are included in the heat transport. An oceanic GCM with a horizontal resolution as coarse as used for the CSU atmospheric GCM can not reproduce these features.

The seasonal change of the uniform heating rate in the deep ocean,

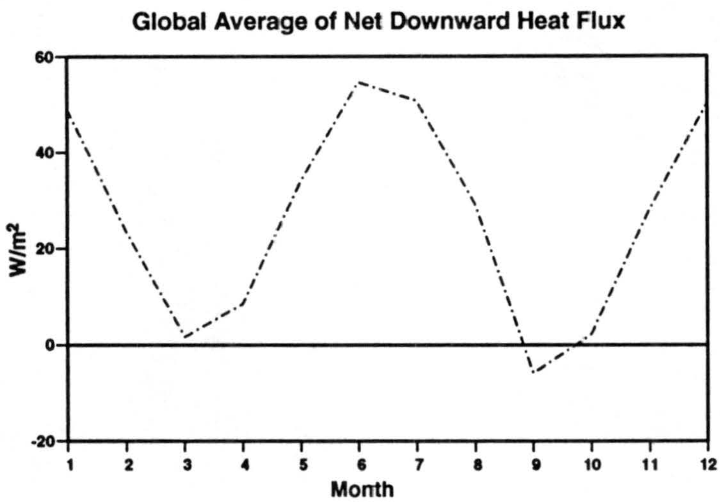

Figure 5: Net heating rate of the deep ocean as function of month. It has been assumed that this rate is spatially uniform. Units are W/m^2.

$\partial[E_d]/\partial t - Q_o$ is shown in Fig. 5. Note that the uniform flux correction predicted from the control run is included here.

2.3 Two Layer Upper Ocean Model

We use a one-dimensional two-layer ocean. The mixed layer depth h is taken from observations. The heat content in the mixed layer is

$$E_1 = \rho_w c_w T h \tag{14}$$

where ρ_w is the density, c_w the heat capacity of sea water and T the mixed layer temperature. The heat content of the water between the mixed layer and its annual maximum is

$$E_2 = E_u - E_1, \tag{15}$$

(see Fig. 6). When the mixed layer detrains E_2 changes according to

$$\frac{\partial E_2}{\partial t} = -\rho_w c_w T \frac{\partial h}{\partial t} \tag{16}$$

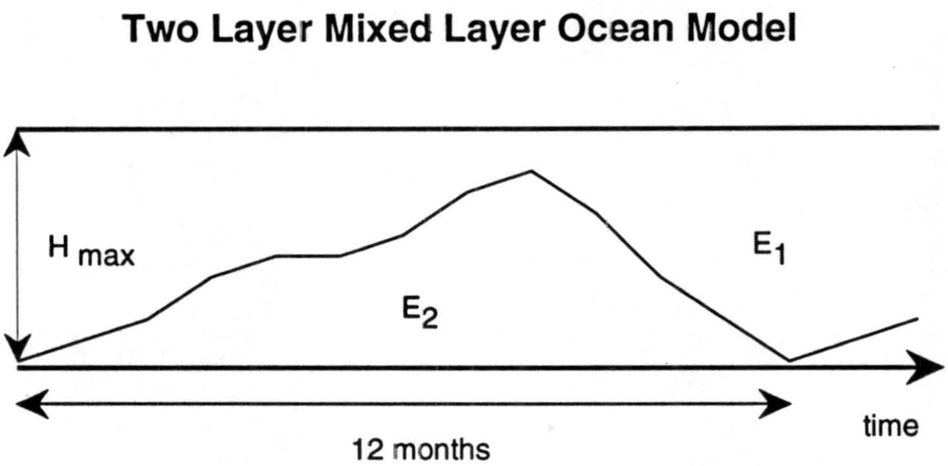

Figure 6: Ocean energy content in two-layer model.

and during entrainment when the mixed layer deepens,

$$(h_{max} - h)\frac{\partial E_2}{\partial t} + E_2\frac{\partial h}{\partial t} = 0. \tag{17}$$

For both cases an Euler forward time integration scheme is used. There is thus full mixing in the second layer. The mixed layer temperature is calculated from the energy balance

$$\rho_w c_w \frac{\partial Th}{\partial t} = (F + Q - \frac{\partial E_2}{\partial t}) \tag{18}$$

where Q is the prescribed heat transport determined from the control run. F is the net atmospheric heat flux calculated using bulk formulae during coupled experiments. The finite difference form of (18) is

$$T^{n+1} = T^n h^n / h^{n+1} + \frac{\Delta t}{\rho_w c_w h^{n+1}}(F + Q - \frac{\partial E_2}{\partial t})\Big|^{n+1/2} \tag{19}$$

where $n+1$ is the new time level. As mentioned earlier, the quantity Q on the right hand side is prescribed in time. The finite difference formulations of (16) and (17) are

$$\frac{E_2^{n+1} - E_2^n}{\Delta t} = -\rho_w c_w T^n (h^{n+1} - h^n)/\Delta t \tag{20}$$

and

$$E_2^{n+1} = \frac{(h_{max} - h^{n+1})}{(h_{max} - h^n)} E_2^n \tag{21}$$

respectively.

2.4 Alternative Ocean Model

The ocean model formulation above has a prognostic second layer heat content, E_2, but assumes full mixing in that layer. If mixing does not take place, it is necessary to know the temperature profile between the mixed layer and its annual maximum.

During detrainment, when the mixed layer gets shallower, the temperature profile below is "frozen", it i.e. is undisturbed, under the assumption that no mixing occurs below the seasonal thermocline. During entrainment when the mixed layer deepens, the temperature profile is eroded down to the new mixed layer depth. The temperature profile below is undisturbed. This approach is not feasible for a simple Q-flux model. One option is to use $\partial E_2/\partial t$ predetermined from a control run and observed SST and $h(t)$. During detrainment, E_2 is calculated as before. During entrainment the heat content below the mixed layer can be computed as

$$E_2^{n+1} = E_{02}^{n+1} \frac{E_2^n}{E_{02}^n} \tag{22}$$

where the index 02 refers to the heat content E_2 during a control run. If E_2, for instance is 10 % higher than during the control run, it remain 10% higher until the maximum mixed layer depth is reached. At that time E_2 is zero by definition. This method ensures that heat from an unusual warm spring will be released gradually during the fall. However, the timing may be lost. Heat is released at the same rate as during a control run, assuming that the temperature profiles are proportional. If the temperature profile had been saved, excess heat stored in the seasonal thermocline in the early spring should not be released until late in the fall under the assumption that no mixing occurs in the seasonal thermocline. The method applied above adds mixing (or unmixing) below the thermocline since it relies on similarity of the temperature profiles between the coupled run and the control run.

2.5 Monthly Observed SST

The atmospheric model control run was done with SST varying linearly from month to month. While this choice seems very reasonable, it involves some consideration to avoid inconsistencies when the mixed layer is added. Equation (3) is used to calculate E_u in general, but since $T(0)$ varies linearly with different rates, E_u becomes pointwise non-differentiable. Consider the detrainment case. By definition (15), we have

$$\frac{\partial E_u}{\partial t} = \frac{\partial E_1}{\partial t} + \frac{\partial E_2}{\partial t} \tag{23}$$

Using (14) and (16), we find

$$\frac{\partial E_u}{\partial t} = \rho_w c_w [\frac{\partial (hT)}{\partial t} - T\frac{\partial h}{\partial t}] = \rho_w c_w h \frac{\partial T}{\partial t} \tag{24}$$

where T and h is the mixed layer temperature and depth, respectively. If the temperature varies linearly with the rate ξ, we find from (6)

$$Q + F(t) = \frac{\partial E_u}{\partial t} = \xi h(t) \tag{25}$$

The rate ξ is usually a different constant before and after the monthly temperature is updated, so Q becomes discontinuous at the time when ξ is changed. This happens independently of the structure of $F(t)$ or $h(t)$. In other words, if we obtain F from the control run with linearly varying SST's, we need to apply a discontinuous Q in (18) and (19) in order to regenerate the SST's from the control run. For this reason, we found it necessary to store daily means of downward fluxes from the control run. Using least-squares, this data is fit to a piecewise continuous linear function defined by values at the 15th of each calendar month with the annual mean preserved. This net flux function is used (along with ice and SST defined at the 15th of each calendar month and interpolated) to calculate daily values of Q. A similar least squares fit is done to create a monthly Q data set with a preserved annual mean. Climatology is used to initialize the surface temperature and ice thickness for the coupled run, while Q is interpolated each ocean/seaice time step from monthly values.

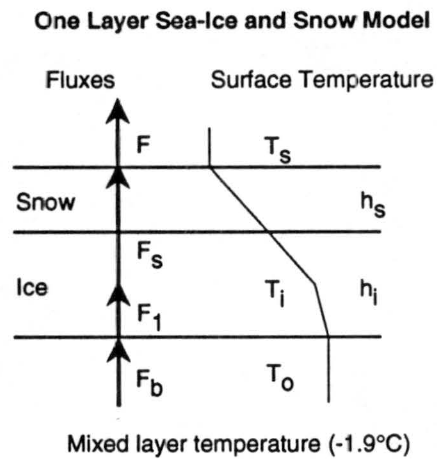

Figure 7: Thermodynamic sea ice and snow model.

2.6 Thermodynamic Sea Ice Model

When the mixed layer temperature predicted by the mixed layer model reaches the freezing point for sea water, further cooling is used to create sea ice. We have adopted a modified version of the thermodynamic model described by Semtner (1976). The sea ice model has a single layer of ice that allows accumulation of snow (Fig. 7). The snow has no heat capacity.

Sea ice forms when cooling predicts a SST below $T_o = -1.9$°C. In that case, the mixed layer temperature is cooled to T_o, while the additional heat flux from the ocean $\delta\mathcal{F}$ is used to create a thin ice layer of thickness h_i, given by

$$h_i = \Delta t \; \delta\mathcal{F}/q_b \tag{26}$$

where Δt is the time step and $q_b = \rho_i L$ is the heat of fusion. The surface temperature T_s of the sea ice is set to the freezing point T_o. Within a grid box the sea ice thickness is assumed uniform without leads. When ice is present, the change, ΔT, in ice surface temperature, T_s, is calculated from a Taylor expansion (in T_s) of the heat flux balance at the top of the ice, i. e.

$$(1-\alpha_s)(1-I_o(1-\Theta(h_s)))S^{\downarrow}+F^{\downarrow}+H+LE-\sigma T_s^4-4\sigma T_s^3\,\Delta T+F_s=0 \tag{27}$$

where the five first terms are downward short wave and long wave radiation, sensible and latent heat flux and upward long wave radiation, respectively.

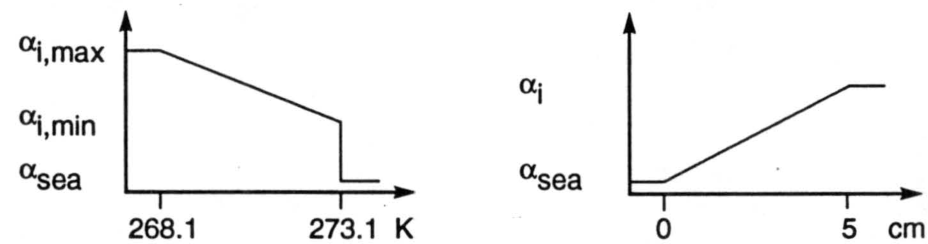

Figure 8: Sea ice albedo

Here α_s is the surface albedo, while the step function Θ ensures that a fraction I_o of the downward solar penetrates into the sea ice only when snow is absent, *e.g.* snow thickness $h_s = 0$. We allow 17% penetration of solar radiation. The sea ice albedo depends on the surface temperature as well as sea ice thickness as shown in Fig. 8. The heat flux through the snow and upper half of the sea ice, F_s, is given by

$$F_s = \frac{T_i - T_s - \Delta T}{h_s/k_s + h_i/(2k_i)}. \tag{28}$$

Here T_i is the sea ice temperature. As long as sea ice is present, the predicted surface temperature is limited to values lower than 0°C. Each time step, a balance surface temperature is predicted to be

$$T_s^* = T_s^n + \Delta T \tag{29}$$

while the predicted surface temperature is limited by

$$T_s^{n+1} = \max\{T_s^*, T_o\} \tag{30}$$

If T_s^* is above freezing, the net incoming heat flux F is calculated as

$$F = (1 - \alpha_s)(1 - I_o(1 - \Theta(h_s)))S^{\downarrow} + F^{\downarrow} + H + LE - \sigma T_o^4 \tag{31}$$

In that case, the resulting flux imbalance at the surface will first melt snow according to

$$\Delta h_s = \Delta t(F - F_s)/q_s. \tag{32}$$

When all snow is melted, the remainder of the surface heat flux, δF is used to melt sea ice:

$$\Delta h_i = \Delta t(\delta F - F_s)/q_i. \tag{33}$$

Here q_s and q_i are the heat of fusion for snow and pure ice (no salt). At the lower boundary a flux imbalance between the heat flux through the bottom half of the sea ice and the heat flux from the mixed layer to the ice, F_b, will result in ablation or accretion of ice. The change in ice thickness is

$$\Delta h_b = \frac{\Delta t}{q_b}\left[\frac{T_o - T_i}{h_i/(2k_i)} - F_b\right] \tag{34}$$

where q_b is the heat of fusion for sea ice with 0.4% salt. Note that the heat of fusion at the lower and upper boundaries of the ice have slightly different values to allow for different contents of liquid brine, (Maykut and Untersteiner, 1971). Most previous studies keep the flux F_b constant. In some of our initial model test runs, we used $F_b = 8\mathrm{W/m}^2$ in Arctic regions and $25\mathrm{W/m}^2$ in Antarctic regions. In a recent study, Fichefet and Gaspar (1988),the oceanic heat flux was allowed to vary due to entrainment and diffusion from below the mixed layer, absorption of transmitted solar irradiance and changes in the freezing point because of salt fluxes. Since we use a prescribed oceanic heat transport Q we compute the oceanic flux to the ice as

$$F_b = Q - \frac{\partial E_2}{\partial t} - \rho_w c_w T \frac{\partial h}{\partial t} \tag{35}$$

in analogy to the form suggested by Fichefet and Gaspar (1988). This formulation ensures that energy is conserved.

The sea ice temperature is calculated by a flux imbalance in the center of the ice layer

$$\rho_i c_i h_i \frac{dT_i}{dt} = F_1 - F_s + (1-\alpha_s)I_o(1-\Theta(h_s))S^{\downarrow} + \rho_i c_i h_i \frac{\Delta h_b \Theta(\Delta h_b)(T_b - T_i)}{\Delta t(h_i + \Delta h_b \Theta(\Delta h_b))} \tag{36}$$

Here c_i is the heat capacity of sea ice. The two last terms represent contributions from penetrating solar radiation and accretion of sea ice of temperature T_o, respectively. In contrast to Semtner (1976) who applied an explicit numerical scheme we adopt an implicit backward Euler scheme when calculating the fluxes F_1 and F_s through the snow and sea ice. This allows the layer thickness to approach zero and thus avoids Semtner's use of a 0-layer model without heat capacity for thin sea ice. Since a single sea ice layer is used the numerical calculation of sea ice temperature simply becomes

$$T_i^{n+1} = \frac{T_s + T_o(1+2r) + T_i^* p}{2(1+r)+p} \tag{37}$$

where

$$r = \frac{h_s k_i}{h_i k_s} \tag{38}$$

is the ratio of "heat flux resistance" of the snow to that of the sea ice and

$$p = \frac{\rho_i c_i h_i}{\Delta t}\left(\frac{h_s}{k_s} + \frac{h_i}{2k_i}\right) \tag{39}$$

is a measure of the rate of change in heat storage. The asterisk on T_i implies a correction to the temperature due to penetrating solar radiation and due to conservation of heat, when new sea ice of temperature T_o is accreted at the bottom. The corrected temperature is given by

$$T_i^* = \frac{\Delta t}{\rho_i c_i h_i}(1-\alpha_s) I_o (1-\Theta(h_s)) S^{\downarrow} + \frac{T_i h_i + T_o \Delta h_b \Theta(\Delta h_b)}{(h_i + \Delta h_b \Theta(\Delta h_b))} \tag{40}$$

The snow is assumed to have zero heat capacity in this formulation. Another difference from Semtner (1976) is that heat from penetrating solar radiation is applied instantly to increase the sea ice temperature instead of potentially being stored in "brine pockets" for sea ice near 0°C. Since our sea ice temperature usually is near the freezing point, T_o, of sea water, the heat release would be instantaneous if a formulation similar to Semtner's was applied. For thin snow-free ice the sea ice temperature simply becomes an average of the surface temperature T_s and the ocean mixed layer temperature T_o.

2.7 One-dimensional Sea Ice Simulations

Figure 9 shows the results of three 15-years simulations using prescribed monthly atmospheric fluxes similar to those used by Semtner (1976). The mixed layer depth, which is only relevant during ice free periods in the case of prescribed F_b, was chosen to be 30 m, which is typical for summer conditions. The same climatological forcing is repeated for each of the 15 years.

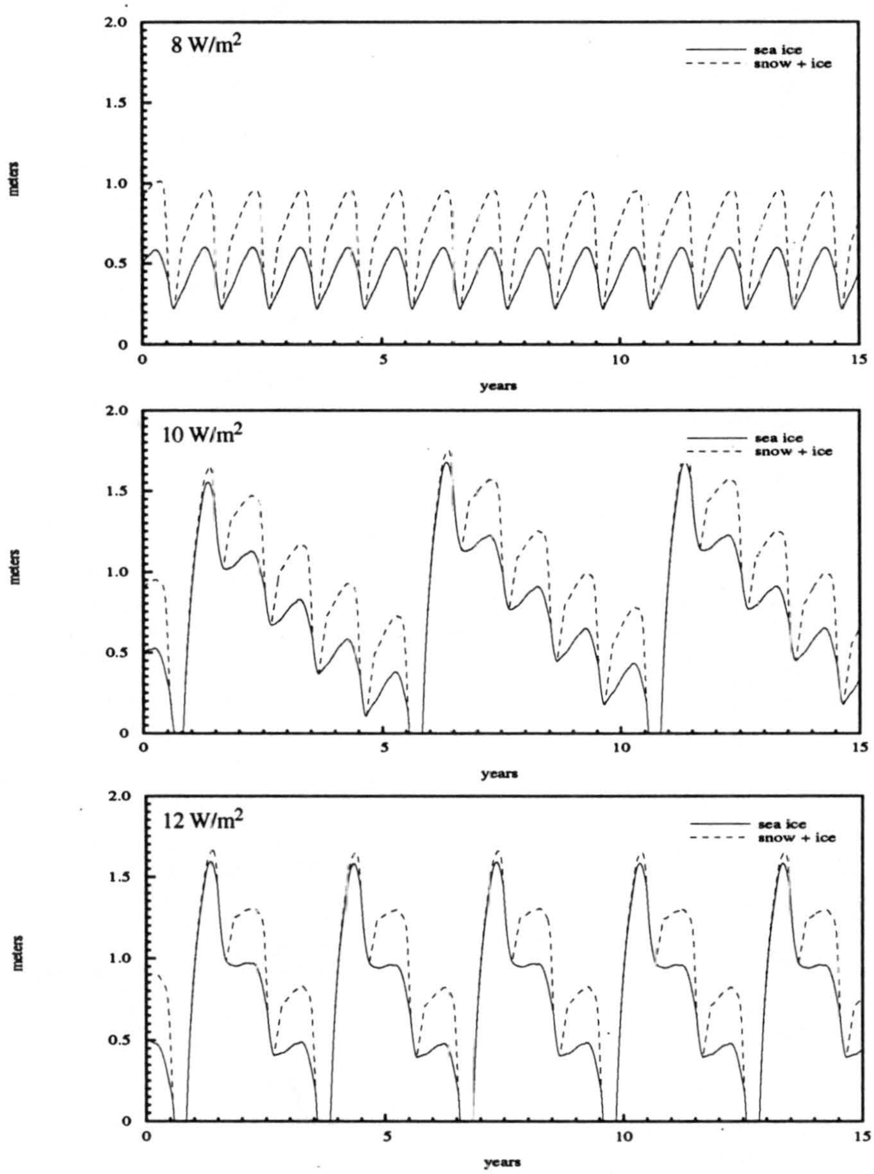

Figure 9: Variation in sea ice and snow thickness predicted by a 15 year integration of the one-layer thermodynamic model for 3 different values of heat flux from the ocean mixed layer. Units are meters.

For $F_b = 8$ W/m^2 we get an average ice thickness of 0.4 m with an annual amplitude of 0.2 m. The snow cover varies annually between 0 and 0.9 m. By increasing the oceanic heat flux to 10 W/m^2, open water appears every 5 years and ice thickness up to 1.5 m appears. Increasing F_b by an additional 2 W/m^2, the quasi-period is shortened to 3 years. In the model cases with open water, early snow fall before sea ice is formed and less snow is accumulated than in years when the sea ice remains during all seasons. Due to less insulation of a thinner snow cover, rapid sea ice growth follows an open water event. As a result multi-year cycles of sea ice coverage may occur even in this simple model. The period between open water events depends on the flux balance between the atmosphere and ocean.

3. CLIMATE SIMULATIONS

The simple model described here should only be considered a first step away from prescribing SST, but is a computational efficient way to include a limited SST response to global warming. Since the climate perturbations supposedly are small, it is reasonable to use the oceanic heat convergence from the control run and observed mixed layer depths.

Coupling to the atmosphere is through surface heat fluxes for both models. When forced by atmospheric history tapes from the 10 year control run, the simple model, with prognostic heat flux, reproduces the observed SST without trends for at least 10 years. This semi-coupled run was used to calibrate the model.

Details about the coupling to the atmospheric model are presented in this section. Two cases are discussed below. One, called the semi-coupled model, uses history tapes from the control run to force the ocean mixed layer model, while the second is a fully coupled model. The former is used to ensure stability and that no trends are present in the ocean mixed layer model and the air-sea interaction scheme.

3.1 Semi-Coupled Model

From a 10-year run using observed monthly SST, (1979-1988) we obtain 365 multi-year daily means of the following quantities: ventilation mass flux, V_m; total precipitation; surface pressure, p_s; surface temperature, T_s; net downward solar radiation at the surface, $S' \downarrow$; downward component of long wave radiation at the surface, $F^{\downarrow}$; atmospheric mixed layer moist static energy, h_m; and atmospheric mixed layer mixing ratio, q_m. These are all needed to force the ocean/sea-ice model. The prime in $S' \downarrow$ indicates that correction for albedo is included. The GCM run had a resolution of 5 degrees in longitude and 4 degrees in latitude with 17 layers in the vertical. Using the method of least-squares, all fields are fit to piecewise-continuous linear functions defined by values at the 15th of each calender month, with the annual mean preserved. Values from this fit are used to calculate daily values of the net downward heat flux

$$F = S'^{\downarrow} + F^{\downarrow} - \sigma T_s^4 - V_m[c_p(T_s - T_a) + L(q_s - q_m)], \tag{41}$$

where the saturation mixing ratio $q_s = q_s(T, p_s)$, depends on the surface temperature and pressure and the mixed layer temperature in the atmosphere is given by

$$T_a = \frac{(h_m - Lq_m)}{c_p}. \tag{42}$$

At the 15th of each month, the monthly mean value of F was stored, and used with the observed (fitted) fields of SST and sea ice to calculate daily values of Q. The resulting Q was subjected to a piecewise linear fit also.

The semi-coupled run was initialized using SST, sea ice thickness and E_2 calculated from the 10 year climatology. Eqns. (3-4) are used to calculate sea ice thickness from sea ice coverage. The mixed-layer/sea ice model was integrated for 8 years driven by interpolated values of Q and heat flux calculated from eqns. (24-25), but now with a prognostic T_s. We found the model to be stable without any climate drift (Fig. 10).

3.2 Model Calibration

The model's main advantage is it simplicity and the very low computational cost. Yet, our results show that it is applicable to climate simulations of several decades. These results are remarkably good, given the well-known tendency of 1-D thermodynamic sea ice models to be noisy and to induce climate drift when coupled to GCM with a daily cycle. The main reason for these problems is that the albedo for sea ice is often modeled like a simple step function dependent on temperature, i.e. high albedo below and low albedo above freezing.

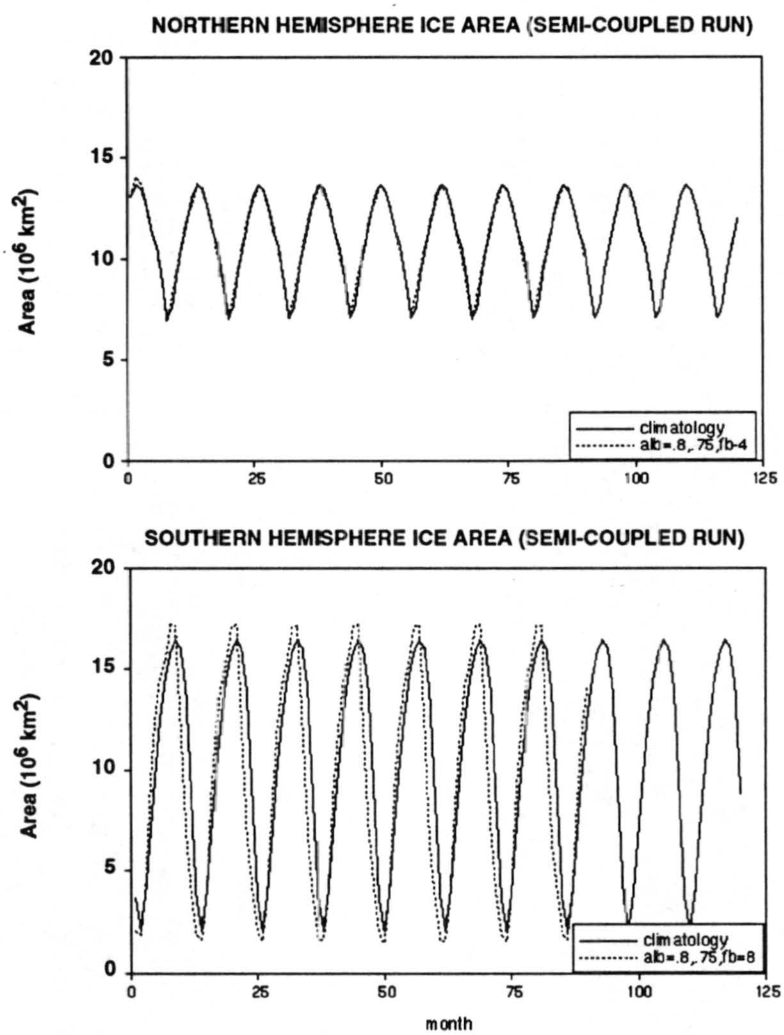

Figure 10: Sea ice areas from an 8-year semi-coupled run with ice albedos of 0.8 and 0.75 for freezing and melting ice and snow, respectively. The heat flux from the ocean was 4 W/m^2 for the Arctic and 8 W/m^2 for the Antarctic oceans.

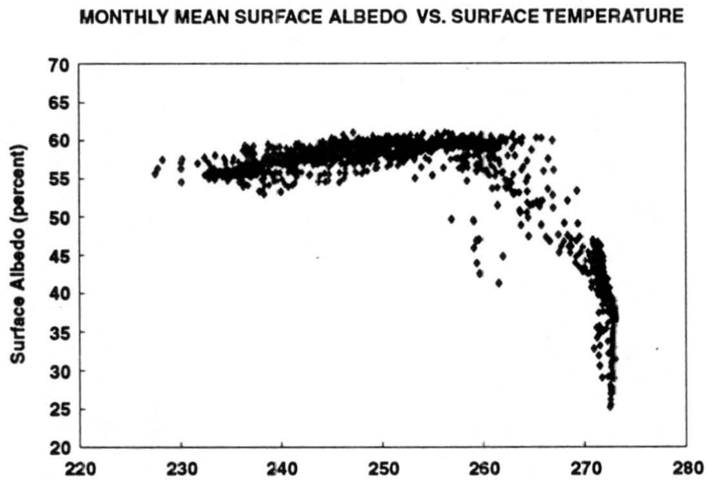

Figure 11: Monthly mean surface albedo versus surface temperature (°K) over sea ice during a semi-coupled run.

Another very important aspect is that the sea ice model requires that the SST has to be at the freezing point whenever sea ice is formed. Observations of SST might be above the freezing point due to presence of leads. In order for the coupled model to be able reproduce an observed SST field it is crucial to lower the observed SST to the freezing point before sea ice appears and to keep the SST at the freezing point until all sea ice has disappeared. This change to the observed SST, should be done before the oceanic heat transport Q is computed (see section 2.1). We have used monthly observed SST and monthly observed sea ice coverage and interpolated linearly from month to month. In that case SST must be kept at the freezing point from one month before sea ice forms to one month after sea ice has disappeared.

We found a high sensitivity to snow and sea ice albedo in the semi-coupled runs, where the air-sea interaction and ocean was forced by history tapes of GCM output. As discussed by Meehl and Washington (1990), this is also found to be these case in other studies using one-dimensional thermodynamic ice models.

For runs with a daily cycle included, we found that the effective surface albedo was lower than anticipated. This is demonstrated in Fig. 11, which shows the corresponding monthly mean albedo for visible light, and the reason is as follows. When the ocean is forced by daily mean values the surface temperature is usually below freezing and the albedo remains high. With a daily cycle, daytime surface temperature above freezing will lower the albedo, to an effective mean value closer to that of melting ice rather than that of frozen ice. Initial tests with the fully coupled model had therefore too much melting in the spring using the original CSU model albedos as above, even with low values for oceanic heat flux. It is clear that the ice cover is highly sensitive to the albedo. A step function with an albedo of 0.6 for freezing ice and 0.36 for melting ice was originally used.

We consequently adopted higher albedos of 0.8 and 0.65 for freezing and melting ice, respectively. These new values were in better agreement with those most commonly used for thermodynamic sea ice models and reported in the literature: Maykut and Untersteiner, (1971); Corby et al., (1977); Parkinson and Washington, (1979); Herman and Johnson, (1980); Hibler and Walsh, (1982);Washington and Meehl, (1984); Ledley, (1985); Shine and Henderson-Sellers, (1985); Mellor and Kantha, (1989);Fleming and Semtner, (1991); Tang, (1991). Details from these studies are shown in Table 1. These new albedos tended to produce too thick sea ice, which only allowed realistic simulations of a few years.

To get a more realistic sea ice albedo for this simple model, which does not take leads in account, we finally adopted an albedo formulation where the albedo varies bi-linearly with temperature and sea ice thickness as shown in Fig. 8. For sea ice thicker than 5 cm, the albedo varies between 0.65 and 0.8 depending on temperature. For thinner sea ice this albedo is reduced linearly towards the open sea albedo. Effectively, it works like an average of the two previous cases, while representing additional physics such as melt ponds and newly formed dark thin ice.

When snow with a constant albedo of 0.8 was allowed to accumulate snow on top of the sea ice we also found our coupled model to become noisy. The main reason is that large fluctuations in albedo and heat flux may occur instantaneously when a single grid cell is covered with a thin, but highly insulating snow cover. In order to get even better simulations, effects such as snow to ice conversion, snow aging and fractional coverage must be included.

Reference	frz snow	mlt snow	frz ice	mlt ice
Fleming and Semtner, 1991	0.80	0.75	0.70	0.70
Tang, 1991	0.75	0.75	0.64	0.64
Meehl and Washington, 1990	0.85	0.60	0.60	0.30
Mellor and Kantha, 1989	0.82	0.73	0.64	0.64
Maykut and Perovich, 1987				0.50
Ledley, 1985	0.88	0.51	0.88	0.51
Shine and Henderson-Sellers, 1985	0.80	0.65	0.72	0.53
Washington and Meehl, 1984	0.80	0.80	0.70	0.70
Hansen et al., 1983	0.85	0.50	0.45	0.45
Hibler and Walsh, 1982	0.75	0.75	0.75	0.66
Wetherald and Manabe, 1981	0.70	0.35	0.70	0.35
Manabe and Stouffer, 1980	0.70	0.45	0.70	0.45
Herman and Johnson, 1980	0.70	0.70	0.70	0.70
Parkinson and Washington, 1979	0.75	0.75	0.75	0.5
Corby et al,, 1977	0.80	0.50	0.80	0.50
Maykut and Untersteiner, 1971	0.83	0.64	0.64	0.64

Table 1. Albedos from other model investigations. The abbreviations "frz" and "mlt" are for "freezing" and "melting", respectively. In several of the models above, the albedo depends on parameters such as temperature, spectral component of the radiation, snow age or latitude.

3.3 Fully Coupled Model

We calculate the oceanic heat transport Q as outlined above and initialize the SST, sea ice thickness and E_2 from the end of a 8 year run with a climatological monthly SST and sea ice obtained as the average from 1979 to 1988 of the Atmospheric Modelling Intercomparison Project (AMIP) data set. The version CSU GCM which was used is described in Randall and Pan, (1993); Fowler et al., (1996) and Randall et al., (1996). The spatial resolution was 9.0° in longitude and 7.2° in latitude with 9 layers in the vertical.

The mixed-layer ocean and sea ice model have been used for coupled runs with the GCM. Care has been taken to ensure consistency is the formulation of flux calculations to avoid climate drift. However, the coupled runs shown here have a small inconsistency due to interpolation of SST fields and sea ice fields. As described in section 3.2, the SST was kept at the freezing point from one month before sea ice is observed to one month after sea ice has disappeared for the calculation of the oceanic heat transport, Q. Sea ice thickness was interpolated from zero the month before sea ice is observed to 1 m in the month it is actually is observed. This procedure avoids spikes in the Q field, but also assumes a slightly colder climate by artificially lowering SST and increasing albedo during two months per year. In the control, the sea ice was interpolated in exactly the same manner, but SST was interpolated to reach the freezing point in the month where sea ice was observed, but truncated to the freezing point whenever sea ice was present. Consequently, for some areas with seasonal sea ice coverage, the SST was slightly higher during the two months where sea ice was created or melted. Later simulations have shown that the effect of this inconsistency was minor.

We have done two coupled runs: One of present climate conditions and one with an instantaneous doubling of CO2. The methodology is as follows:

a) A climatology data set of monthly sea surface temperature (SST) and sea ice coverage was created from observed SST and sea ice coverage from the AMIP period 1979-1988. The sea ice thickness was assumed to be 1 m, e.g. eqns. (4) and (5) were not applied.

b) An 8 year control integration with this climatological data set prescribed over the oceans was used to compute the net downward heat flux F into the ocean.

c) From the climatological SST and sea ice data, the net downward heat flux from the control and observations of mixed layer depth (NODC data), the oceanic heat transport can be computed during the year.

d) A coupled GCM-ocean model run with present level CO2 serves as a reference and to check that no or little climate drift occurs. This is necessary since we want to avoid flux correction in the coupling between the ocean and the atmosphere.

e) A second coupled run is made to investigate the response to increased CO_2 levels.

In these runs, no snow is permitted to accumulate on the sea ice. This choice was made because the spatially noisy precipitation pattern generated by the atmospheric model. As discussed in section 2.7, a one-dimensional thermodynamic sea ice model produces a thickness of sea ice that is extremely sensitive to snow coverage, so the noisy snowfall pattern created an equally

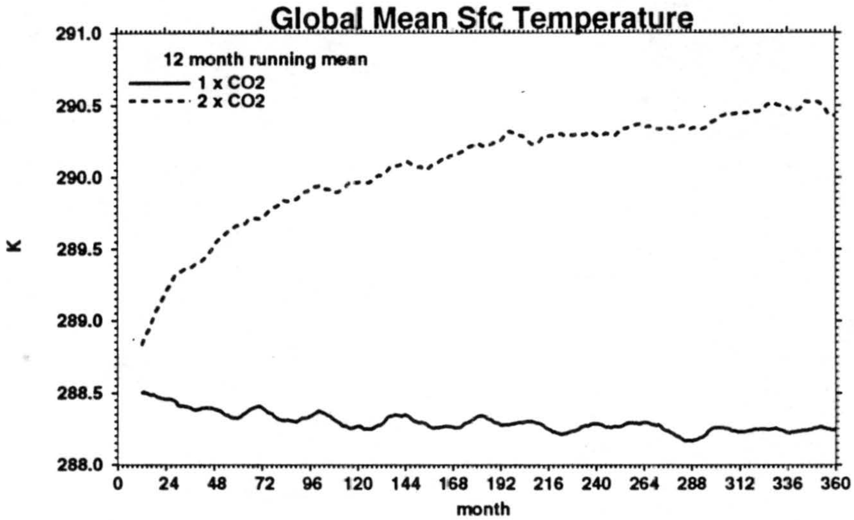

Figure 12: Globally averaged surface temperature during 30 year runs of the GCM coupled to the ocean mixed layer and sea ice model. Units are °K.

noisy sea ice field.

Figure 12 shows the global mean surface temperature for the two coupled 30 year runs. The present day climate simulation has a very small tendency towards a colder climate (about 0.05°C/decade). In comparison we found a 2.3°C increase during the 30 year 2 x CO_2 run.

The areas of sea ice in the northern hemisphere (NH) and southern hemisphere (SH) (Fig. 13) are smaller for the 2 x CO_2 run, in particular for the SH, where the annual sea ice production has been reduced.

This is not surprising, since ice dynamics is more important for the thick multi-year Arctic sea ice, and the oceanic export of 7-10% of the Arctic ice cover through the Fram strait (see Häkkinen, 1990) is not included in our model. Hibler and Walsh, (1982) have also demonstrated the importance of including sea ice dynamics in the Arctic.

3.4 Results from a 2 $\times$ CO_2 run.

In this section fields from the coupled runs are briefly discussed. Figure 14-15 show the SST for February and August, respectively. The control

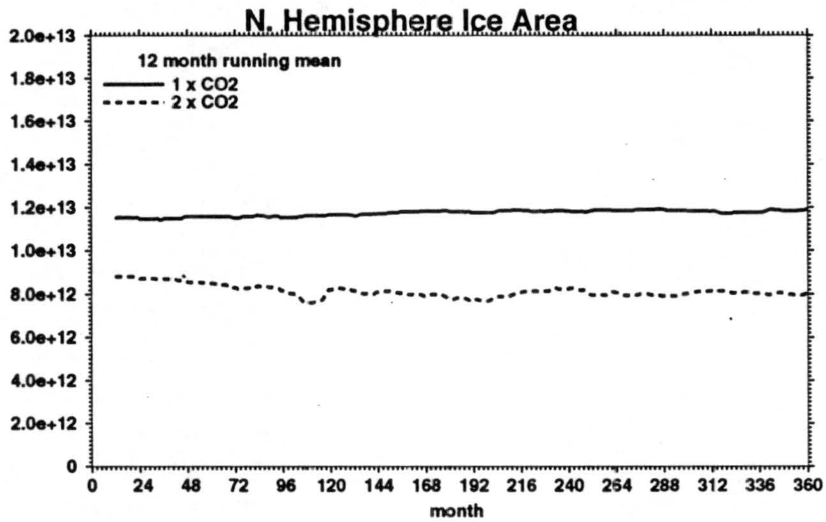

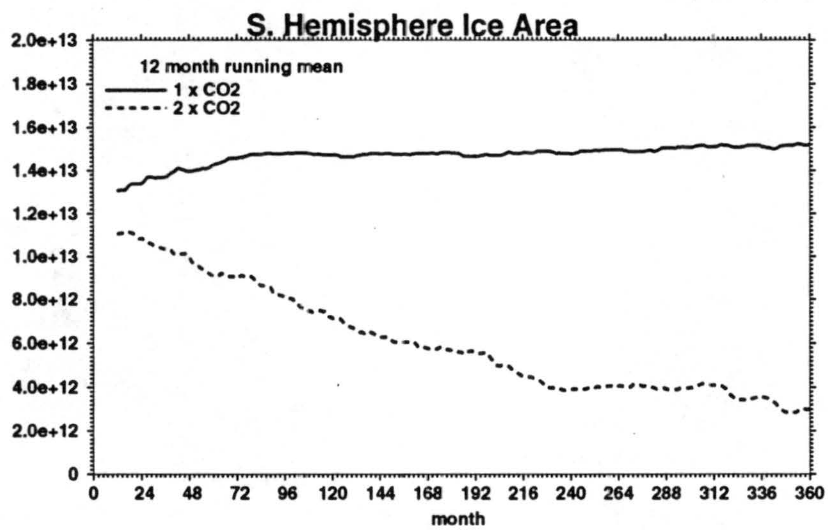

Figure 13: Total sea ice area for the northern hemisphere (top) and southern hemisphere (bottom) for 30 years of coupled runs. Units are m^2.

SST equals observations, since they are prescribed. For the coupled run, the global decrease in SST is about 0.15°C. For example, the area of temperature above 28°C in the tropical Indian and Pacific Oceans is slightly reduced. In contrast, for the instantaneous doubling of CO_2 case, the global SST increase by about 2°C. The increase is larger for the polar regions.

Sea ice coverage (Fig. 16-17) is fairly realistic for the present climate coupled run. This was also indicated by the total area (Fig. 13) during the spin up. However, sea ice thickness tends to be unrealistic. Some grid points accumulate several meters of sea ice which prevents melting during the summer. However, the global effects are presumably fairly small.

Figure 18-19 show total precipitation rates. The changes in these rates for the double CO_2 run are fairly small, only about an 0.1 mm/day increase.

Figure 20-21 show the short wave cloud radiative forcing at the top of the atmosphere. Changes are of the order of a few W/m^2, with largest effect in the polar areas during the summer. For the long wave radiation we find a larger effect, but during the polar winter. This is due to a decreased sea ice extent for the $2 \times CO_2$.

The globally integrated net surface heat flux change is less than 1 W/m^2, which means that the flux correction by a global constant, F_o giving by (10) is justified. As seen from Fig. 22-23 the heat flux mainly changes where sea ice coverage has been reduced.

The amount of precipitable water or water vapor increases by 10%, mainly in the tropical convergence zone (Fig. 24-25).

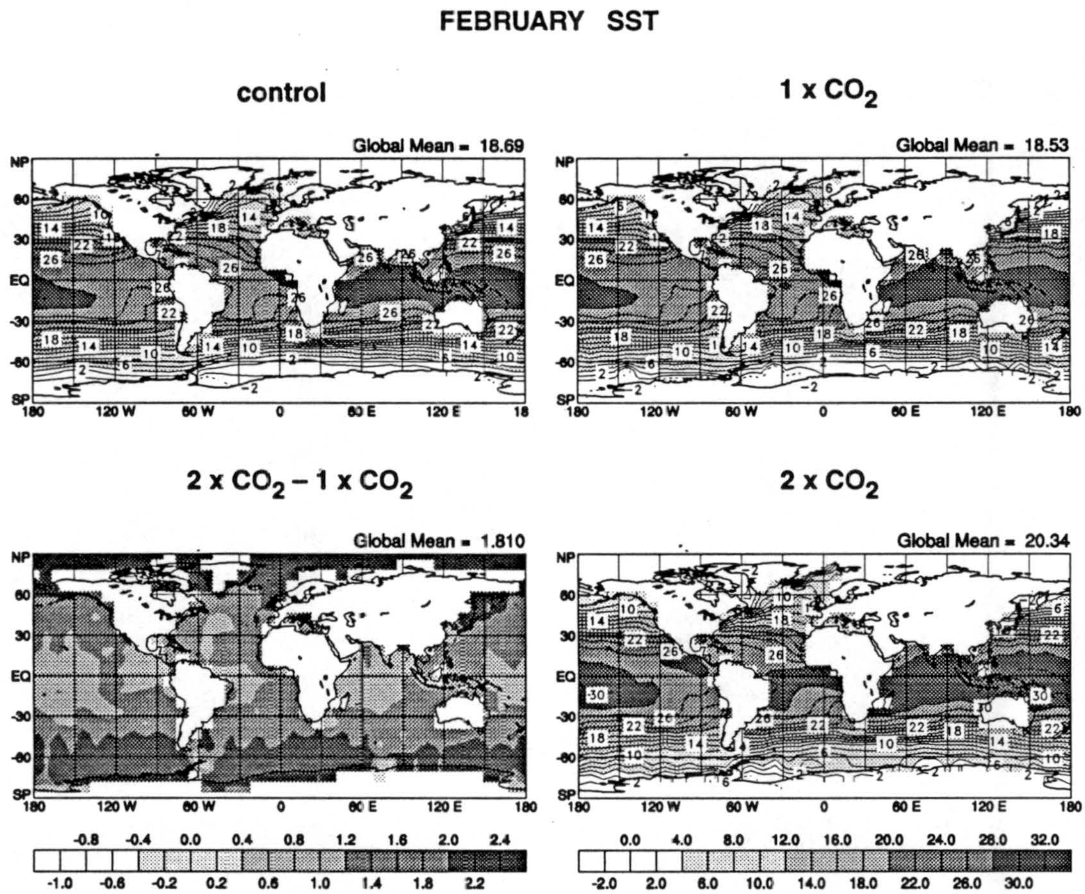

Figure 14: SST for February for the control, 1 × CO_2, 2 × CO_2 and the difference between the two coupled runs. Contour intervals are 2°C.

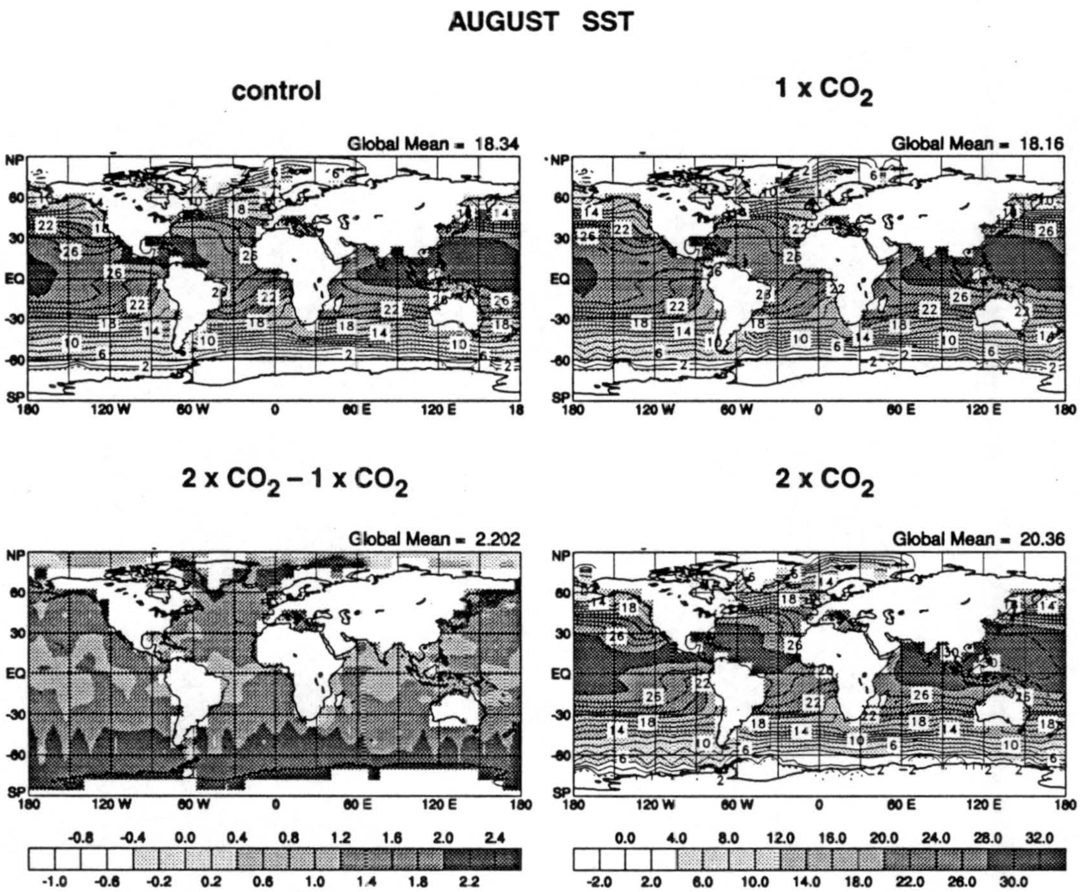

Figure 15: SST for August for the control, 1 × CO_2, 2 × CO_2 and the difference between the two coupled runs. Contour intervals are 2°C.

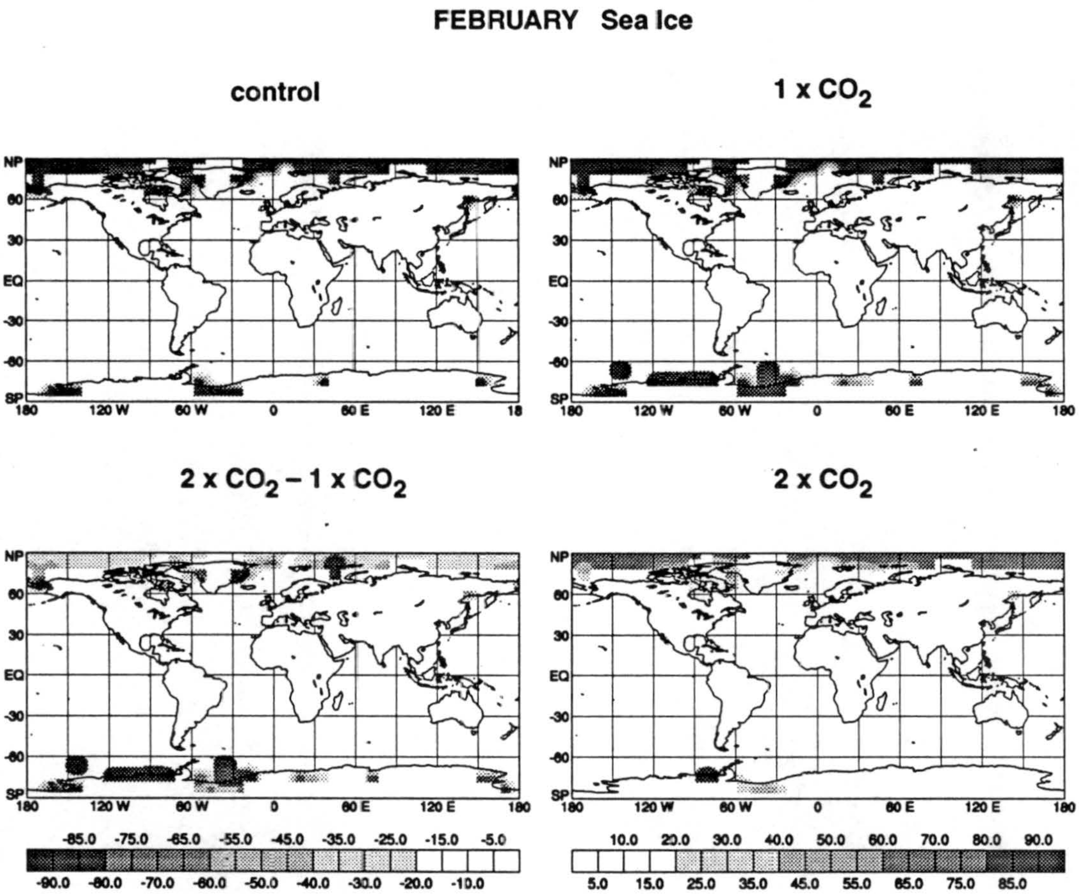

Figure 16: As figure 14, but sea ice thickness. Units are centimeters.

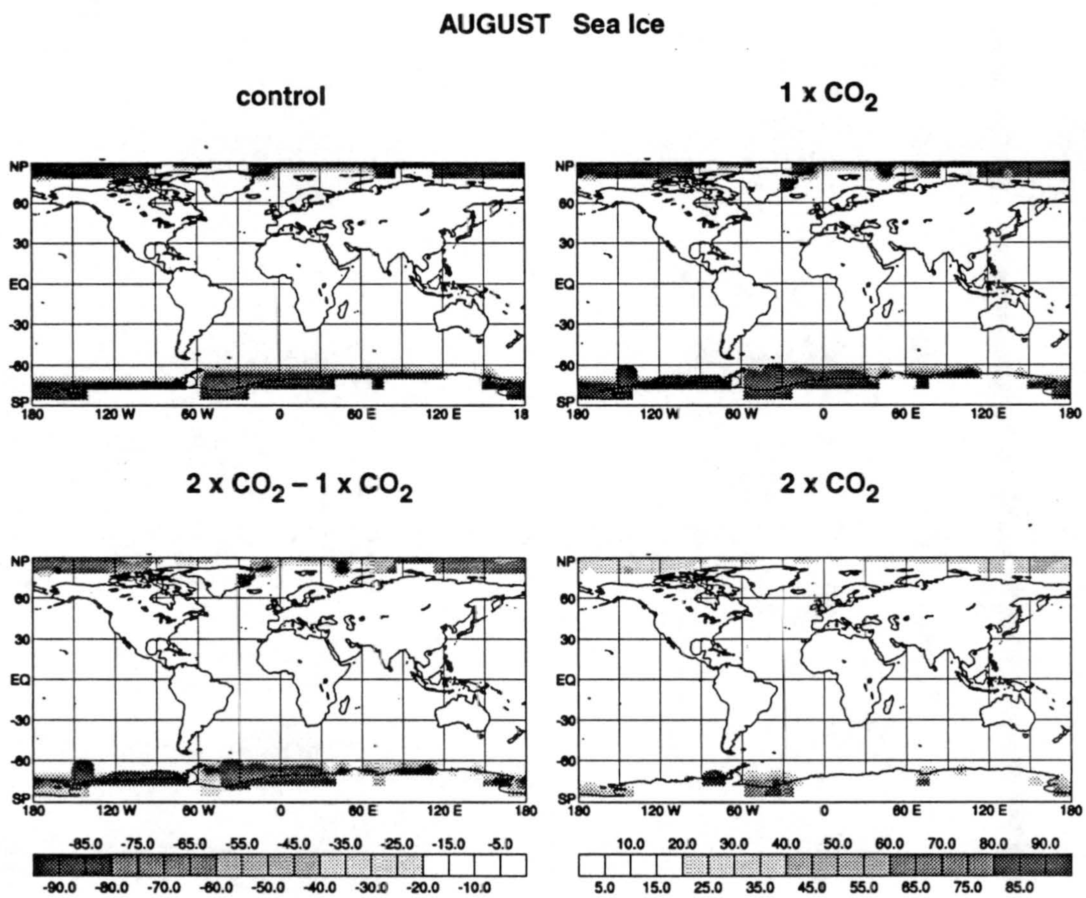

Figure 17: As figure 15, but sea ice thickness. Units are centimeters.

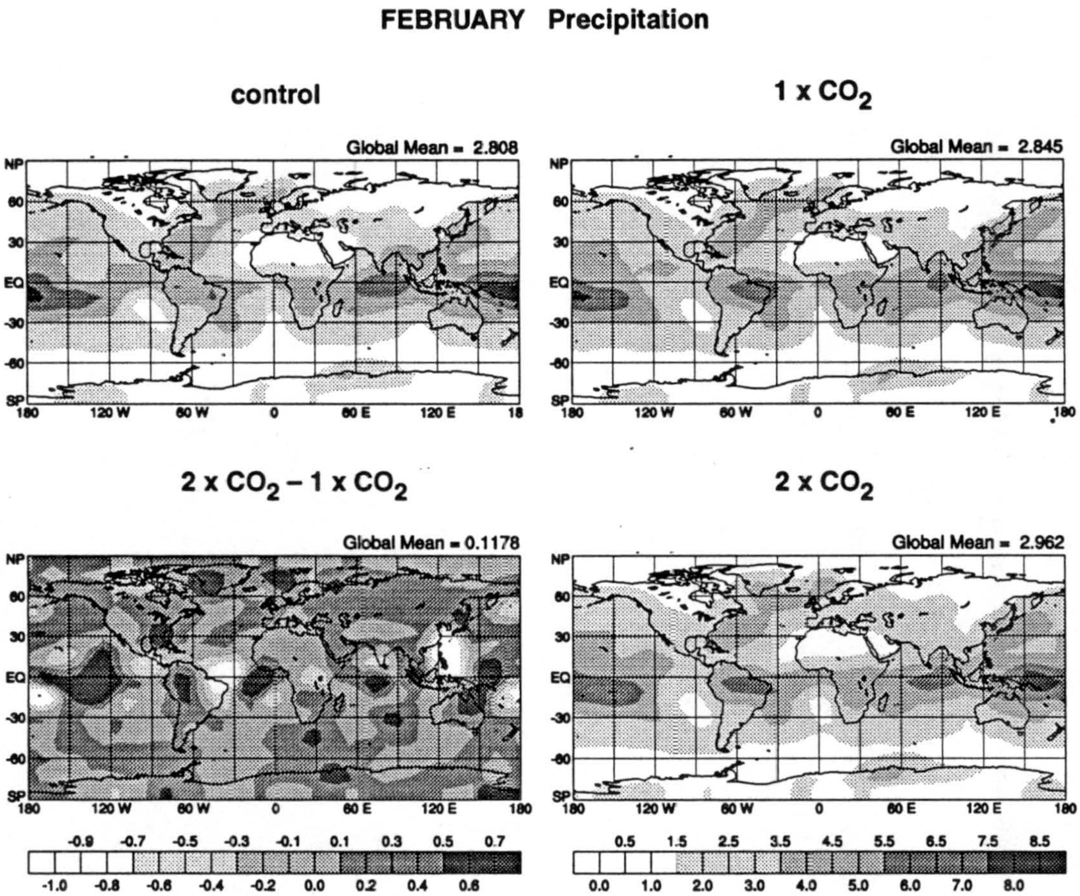

Figure 18: As figure 14, but precipitation rate. Units are mm/day.

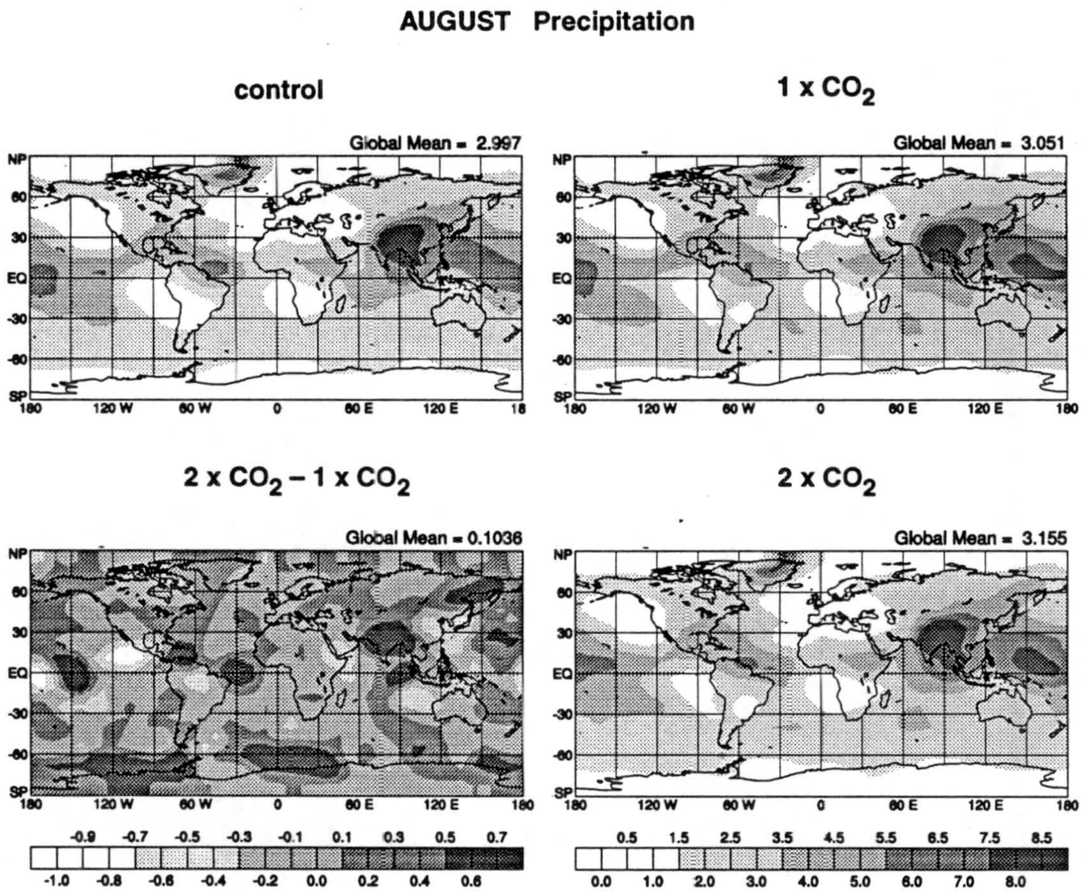

Figure 19: As figure 15, but precipitation rate. Units are mm/day.

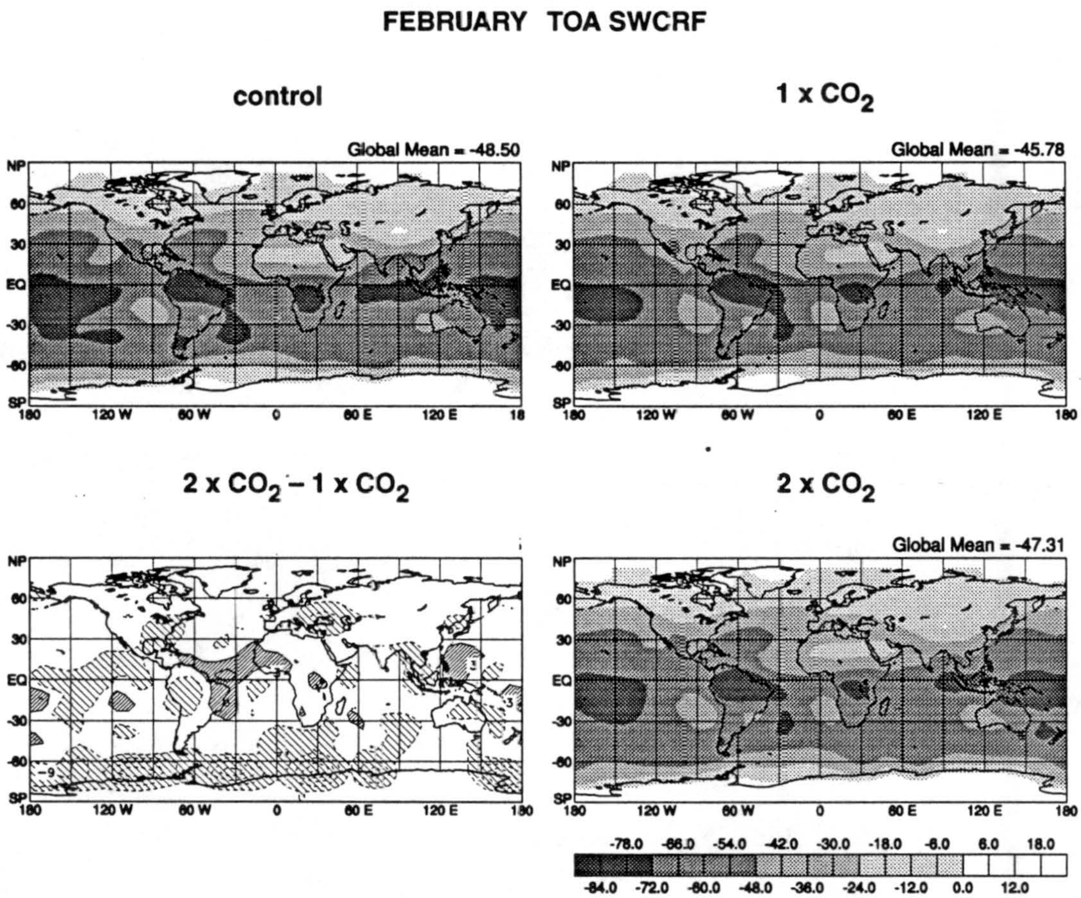

Figure 20: As figure 14, but short wave cloud radiative forcing (top of the atmosphere). Units are W/m^2.

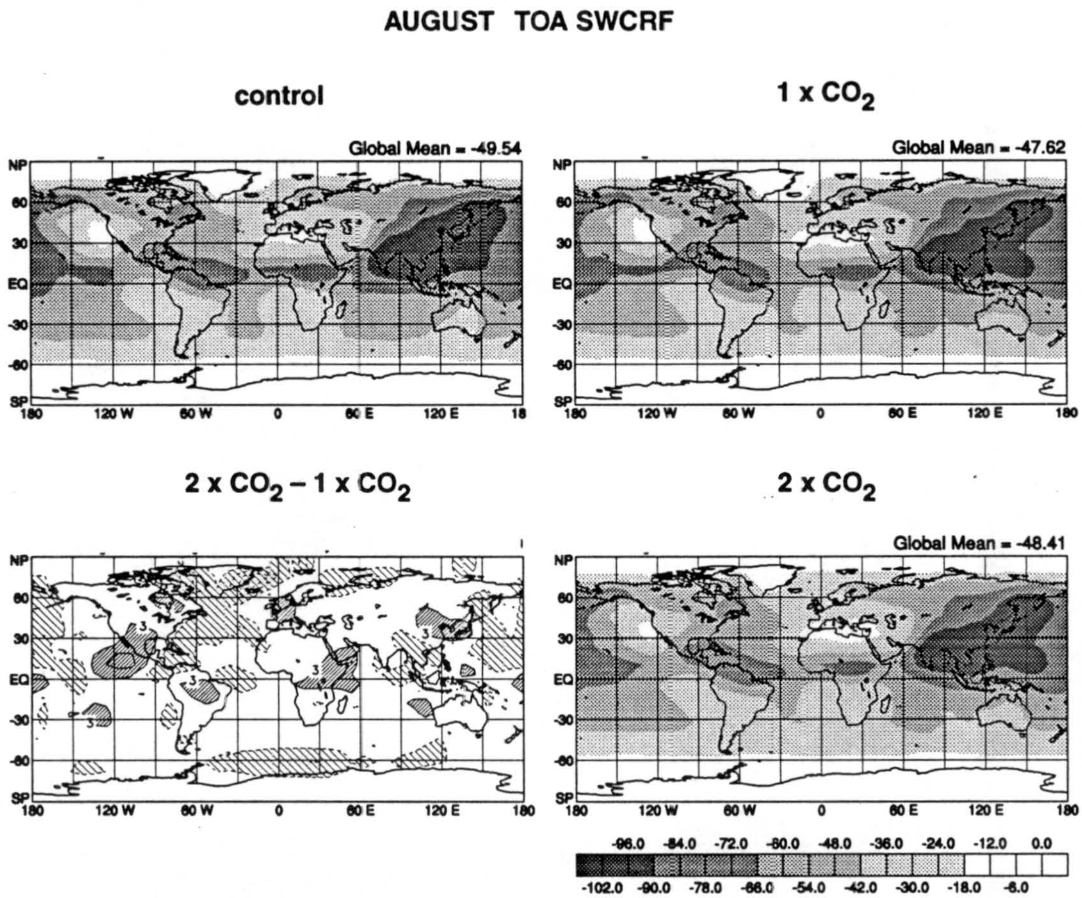

Figure 21: As figure 15, but short wave cloud radiative forcing (top of the atmosphere). Units are W/m^2.

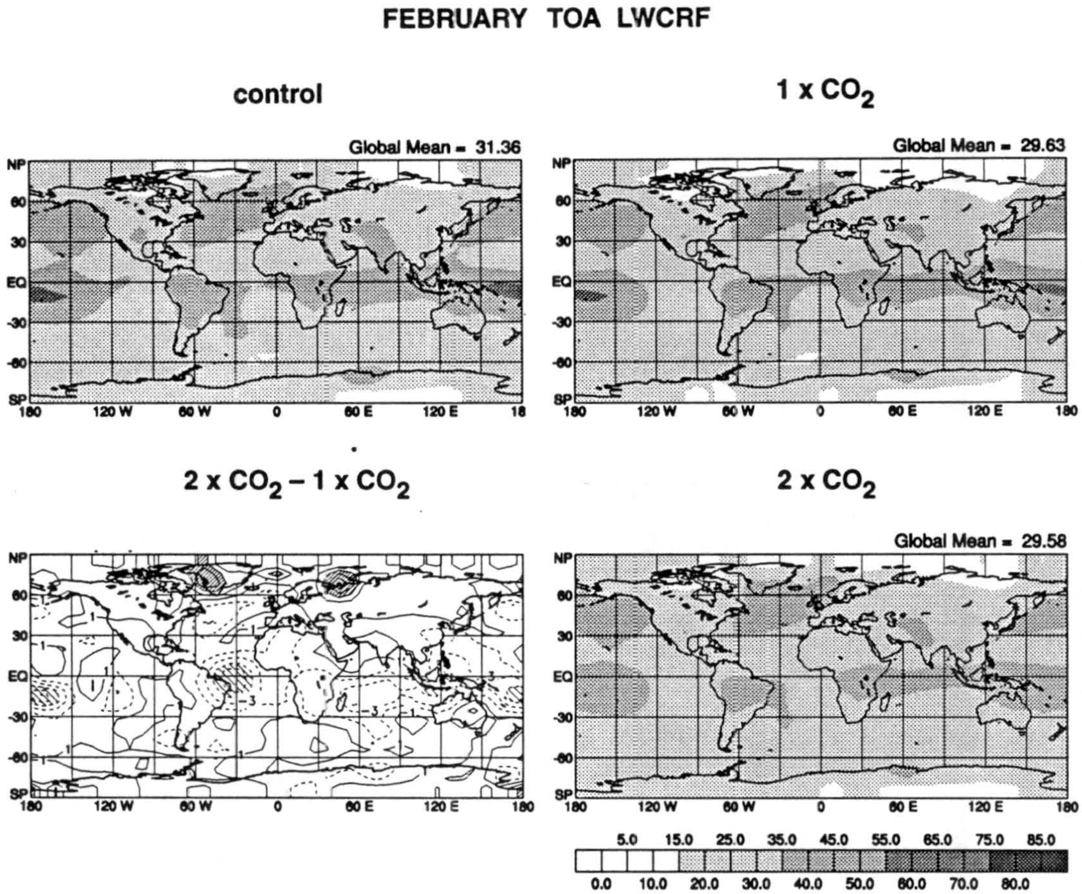

Figure 22: As figure 14, but long wave cloud radiative forcing (top of the atmosphere). Units are W/m^2.

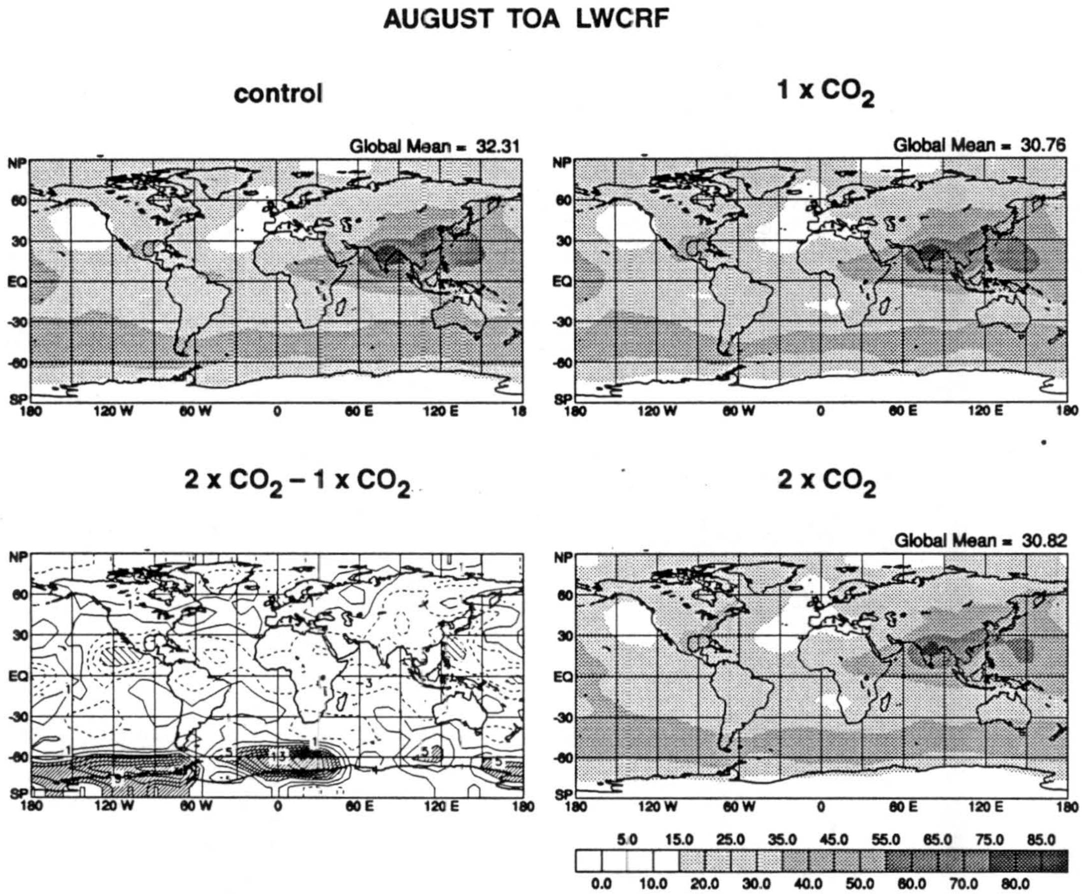

Figure 23: As figure 15, but long wave cloud radiative forcing (top of the atmosphere). Units are W/m^2.

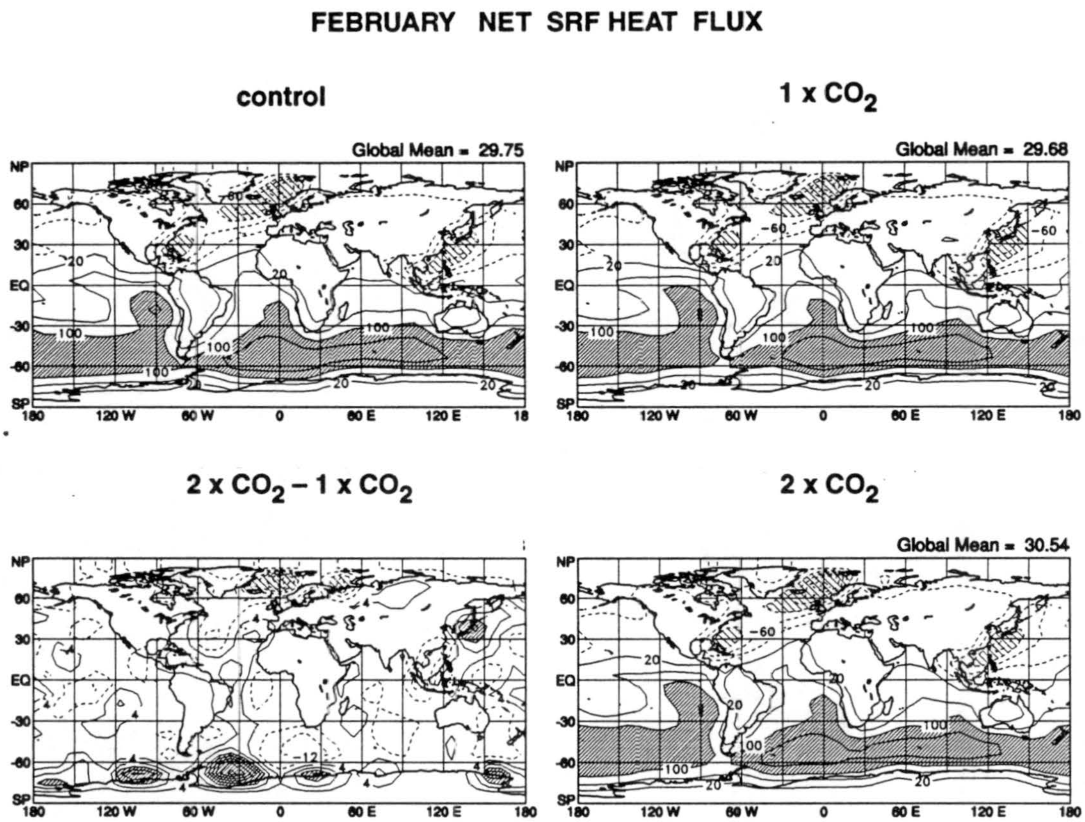

Figure 24: As figure 14, but net surface heat flux. Units are W/m^2.

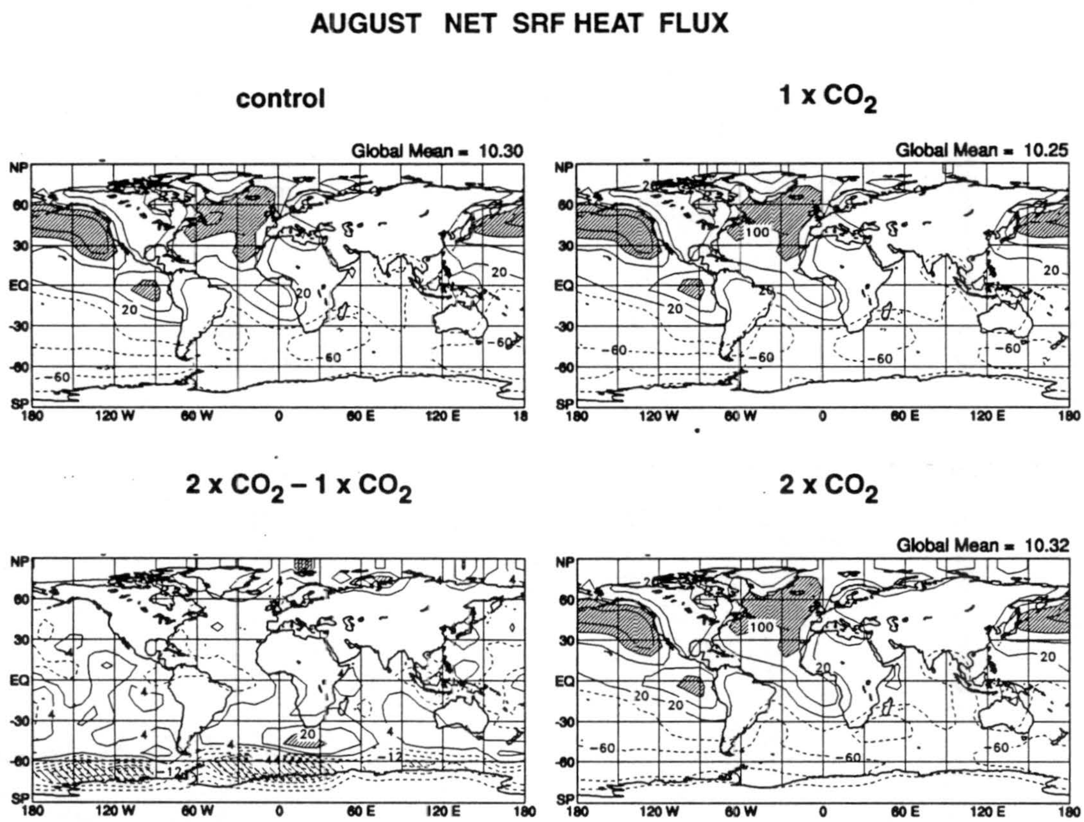

Figure 25: As figure 15, but but net surface heat flux. Units are W/m^2.

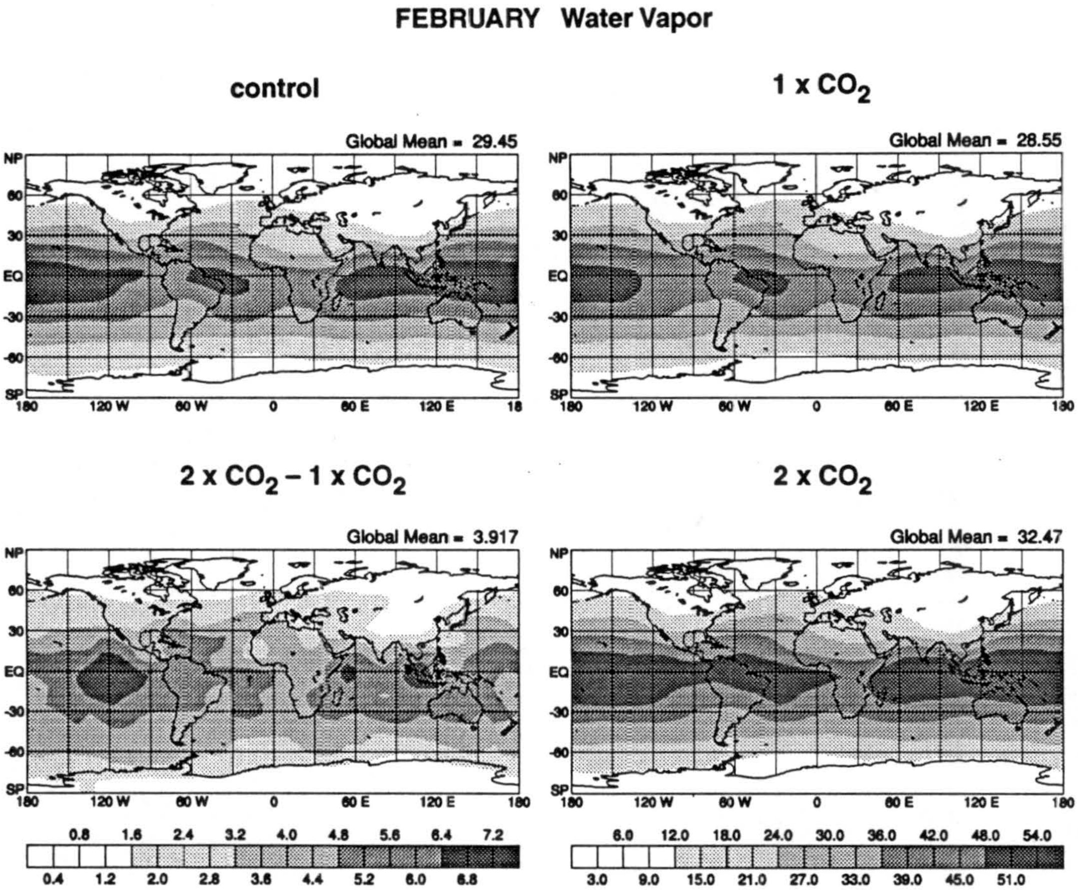

Figure 26: As figure 14, but precipitable water (water vapor). Units are mm.

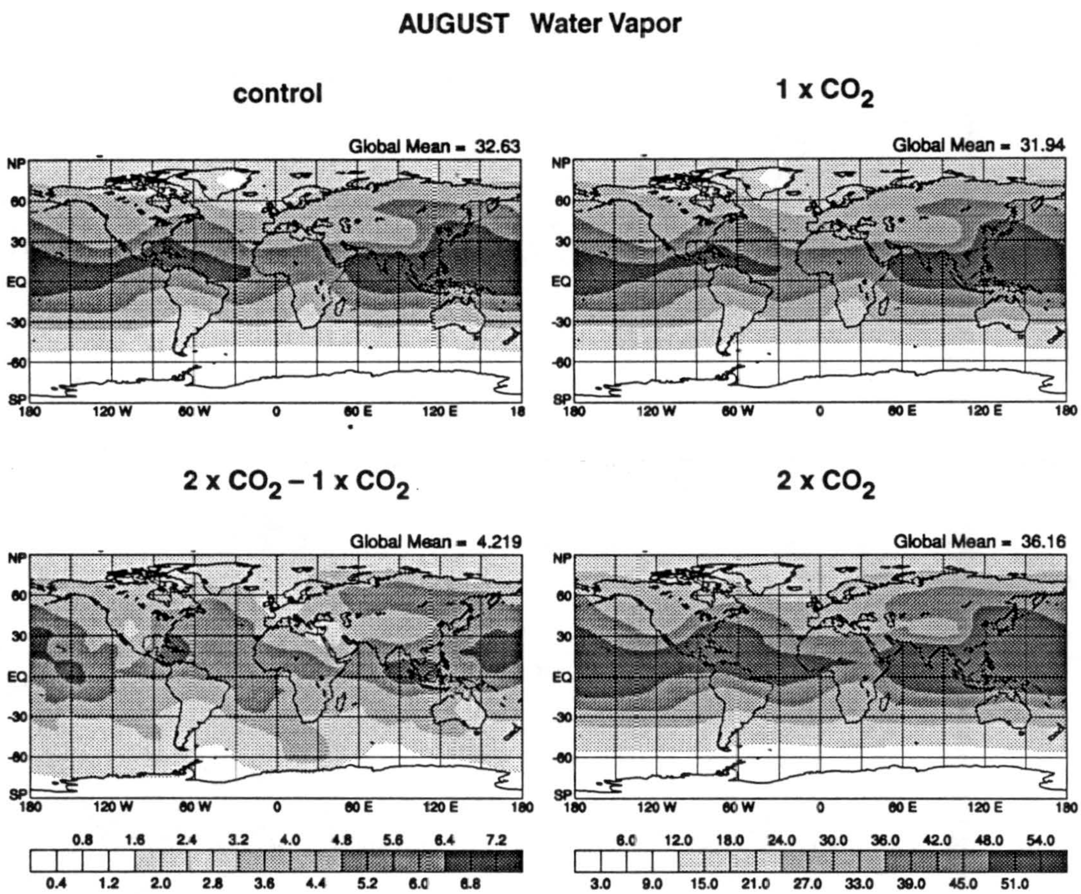

Figure 27: As figure 15, but precipitable water (water vapor). Units are mm.

4. SUMMARY

We have developed and implemented in the CSU GCM a simple two-layer mixed layer model with prescribed oceanic heat transport. Sea ice is included using a thermodynamic one-layer ice and snow model. We have made semi-coupled run in which the state of the atmosphere is prescribed, while the oceanic heat flux, SST and sea ice cover are predicted. Coupled test runs with full interactive atmosphere and ocean have been accomplished. Given the simplicity of the ocean mixed layer and sea ice model, the coupled model show very little climate drift for simulation of current conditions.

5. ACKNOWLEDMENTS

We thank Gary Russell for providing us with ocean data. This work has been supported by grants from the Department of Energy, numbers DE-FG02-89ER69027 and DE-FG03-94ER61929; by a contract from the National Aeronautics and Space Administration, number NAS5-31730; and a subcontract from the University of California Los Angeles, number 0965 G 4A007.

Computing resources were provided by the NASA Center for Computational Sciences and the National Energy Research Supercomputer Center.

6. APPENDIX A

For the purpose of selecting a few harmonics or to apply a filter to a time series, the Fourier transform is needed. Accurate numerical differentiation can also be obtained using a collocation method. For a periodic function, Fourier collocation is adequate and differentiation of a function can be calculated as shown below.

We define the complex discrete Fourier Transform by

$$\tilde{v}_k = \frac{1}{N}\sum_{j=0}^{N-1} v_j e^{-ikx_j}, \qquad k = -N/2, \ldots, N/2-1$$

where $x_j = 2\pi j/N$ and $i^2 = -1$. The inverse or back transform is given by

$$v_j = \sum_{k=-N/2}^{N/2-1} \tilde{v}_k e^{ikx_j}$$

In order to relate the complex Fourier transform as defined to the more familiar cosine and sine transforms, we note that the Fourier coefficients $\tilde{v}_k = r_k + ip_k$ are complex. If v_j is real, the

$$v_j = a_j + ib_j, \qquad b_j = 0, \forall j$$

Then

$$\tilde{v}_k = \frac{1}{N}\sum_{j=0}^{N-1} a_j e^{-ikx_j} = \frac{1}{N}\sum_{j=0}^{N-1} a_j[\cos(kx_j) - i\sin(kx_j)]$$

Thus the real part corresponds to a cosine transform and the imaginary part to a sine transform. We observe that $r_{-k} = r_k$ and $p_{-k} = -p_k$. In order to obtain the cosine transform amplitude A_n and the sine transform amplitude B_n from the complex Fourier coefficients, we use

$$A_k = \tilde{v}_k + \tilde{v}_{-k}, \quad B_k = i(\tilde{v}_k - \tilde{v}_{-k})$$

For a real input series we then have the amplitude C_k and phase Φ_k for a given wave number k given by

$$C_k = \sqrt{A_k^2 + B_k^2}, \qquad \Phi_k = \arctan\frac{B_k}{A_k}.$$

where each harmonic is given by $C_k\cos(kx_j - \Phi_k)$.

For differentiation of a discrete function, the Fourier coefficients $\tilde{v}_k$ are calculated and multiplied by k, viz.

$$\tilde{v}'_k = k\tilde{v}_k, \qquad k = -N/2, \ldots, N/2 - 1.$$

The derivative of the original function is calculated using the inverse transform

$$v'_j = \frac{2\pi}{T}\sum_{k=-N/2}^{N/2-1} \tilde{v}'_k e^{ikx_j}.$$

where T is the (dimensional) period of the time series.

7. REFERENCES

Alexander, R. C. and R. L. Mobley, 1974: Monthly average sea-surface temperatures and ice-pack limits on a 1° global grid. Rep. 4-1310-ARPA, Rand Corp., Santa Monica, 30 pp.

Bryan, K., S. Manabe and R. L. Pacanowski, 1975: A global ocean-atmosphere climate model. Part II: The oceanic circulation. *J. Phys. Oceanogr.* **5**, 30–46.

Corby, G. A., A. Gilchrist, and P. R. Rowntree, 1977: United Kingdom Meteorological Office 5 level general circulation model, *Method. Comput. Phys.*, **17**, 67–110.

Fichefet, Th., and Ph. Gaspar, 1988: A model study of upper ocean–sea ice interactions.*J. Phys. Oceanogr.*, **18**, 181–195.

Häkkinen, S., 1990: Models and their applications to polar oceanography. In: *Polar Oceanography, Part A: Physical Science*, p. 335–384, Academic Press.

Hansen, J., I. Fung, A. Lacis, D. Rind, S. Lebedeff, R. Ruedy and G. Russell, 1988: Global climate changes as forecast by Goddard Institute for Space Studies Three-Dimensional Model. *J. Geophys. Res.*, **93**, 9341–9364.

Hansen, J., A. Lacis, D. Rind and G. Russell, 1984: Climate sensitivity: Analysis of feedback mechanisms. In: *Climate Processes and Climate Sensitivity*, Geophys. Mon. **29**, Am. Geophys. Union, 130–163.

Hansen, J., G. Russell, D. Rind, P. Stone, A. Lacis, S. Lebedeff, R. Ruedy and L. Travis, 1983: Efficient three-dimensional global models for climate simulations: Model I and II. *Mon. Wea. Rev.*, **111**, 609–662.

Herman, G. F., and W. J. Johnson, 1980: Arctic and Antarctic climatology of a GLAS GCM, *Mon. Wea. Rev.*, **108**, 56–68.

Hibler, W. D., and J. E. Walsh, 1982: On modelling seasonal and interannual fluctuations of Arctic sea ice, *J. Phys. Oceanogr.*, **12**, 1514–1532.

Jensen, T. G., D. A. Randall and D. A. Dazlich, 1991: Coupling of the CSU GCM to a simple ocean and sea ice model. *Fifth Conference on Climate Variations*, Denver, American Meteorological Society, 321–322.

Fleming , G. H., and A. J. Semtner, 1991: A numerical study of interannual ocean forcing on Arctic ice. *J. Geophys. Res.*, **96**, 4589-4603.

Fowler, L. D., D. A. Randall, and S. A. Rutledge, 1996: Liquid and Ice Cloud Microphysics in the CSU General Circulation Model. Part 1: Model Description and Simulated Microphysical Processes. *Journal of Climate.* (in press).

Ledley, T. S., 1985: Sensitivity of a thermodynamic sea ice model with leads to time step size, *J. Geophys. Res.*, **90**, 2251-2260.

Manabe, S., K. Bryan and M. J. Spelman, 1975: A global ocean-atmosphere climate model. Part 1: The atmospheric circulation. *J. Phys. Oceanogr.*,**5**, 3–29.

Manabe, S. and R. J. Stouffer, 1980: Sensitivity of a global climate model to an increase of CO_2 concentration in the atmosphere. *J. Geophys. Res.*, **85**, 5529–5554.

Maykut, G. A., and N. Untersteiner, 1971: Some results from a time-dependent thermodynamic model of sea ice. *J. Geophys. Res.*, **76**, 1550–1575.

Meehl, G. A. and W. M. Washington, 1990: CO_2 climate sensitivity and snow-sea-ice albedo parameterization in an Atmospheric GCM coupled to a mixed-layer ocean model. *Climate Change*, **16**, 283–306.

Mellor, G. L., and L. Kantha, 1989: An ice-ocean coupled model, *J. Geophys. Res.*, **94**, 10,937–10,954.

Miller, J. R., G. R. Russell and L.-C. Tsang, 1983:Annual oceanic heat transports computed from an atmospheric model. *Dyn. Atmos. Oceans*, *7*, 95–109.

Parkinson, C. L., and W. M. Washington, 1979: A large-scale numerical model of sea ice. *J. Geophys. Res.*, **84**, 311–337.

Program for Climate Model Diagnosis and Intercomparison, 1990: Atlas of the COLA/CAC AMIP SST and Sea-Ice dataset. UCRL-MA-106632, Lawrence Livermore National Laboratory, University of California.

Randall, D. A., and D. - M. Pan, 1993: Implementation of the Arakawa-Schubert parameterization with a prognostic closure. In: *The Representation of Cumulus Convection in Numerical Models*, K. Emanuel and D. Raymond, Eds., American Meteorological Society, 246 pp.

Randall, D. A., P. J. Sellers, J. A. Berry, D. A. Dazlich, C. Zhang, G. J. Collatz, A. S. Denning, S. O. Los, C. B. Field, I. Fung, C. O. Justice, C. J. Tucker, and L. Bounoua, 1996: A Revised Land-Surface Parameterization (SiB2) for Atmospheric GCMs. Part 3: The Greening of the CSU General Circulation Model. *J. of Climate.* (in press).

Russell, G. R., J. R. Miller and L.-C. Tsang, 1985: Seasonal oceanic heat transports computed from an atmospheric model. *Dyn. Atmos. Oceans*, **9**, 253–271.

Semtner, A. J., 1976: A model for the thermodynamic growth of sea ice in numerical investigations of climate. *J. Phys. Oceanogr.*, **6**, 379–389.

Shine, K. P. and A. Henderson-Sellers, 1985: The sensivity of a thermodynamic sea ice model to changes in surface albedo parameterization, *J. Geophys. Res.*, **90**, 2243-2250.

Tang, C. L., 1991: A two-dimensional thermodynamic model for sea ice advance and retreat in the Newfoundland marginal ice zone. *J. Geophys Res.*, **96**, 4723-4737.

Walsh, J. and C. Johnson, 1979: An analysis of Arctic sea ice fluctuations. *J. Phys. Oceanogr.*, **9**, 580–591.

Washington, W. M., A. J. Semtner, Jr., G. A. Meehl, D. J. Knight and T. A. Meyer, 1980: A general circulation experiment with a coupled atmosphere, ocean, and sea ice model. *J. Phys. Oceanogr.*, **10**, 1887–1908.

Washington, W. M. and G. A. Meehl, 1983: General circulation model experiments on the climatic effects due to a doubling and quadrupling of carbon dioxide concentrations. *J. Geophys. Res.*, **88**, 6600–6610.

Washington, W. M. and G. A. Meehl, 1984: Seasonal cycle experiment on the climate sensitivity due to a doubling of CO_2 with an atmospheric general circulation model coupled to a simple mixed-layer ocean model. *J. Geophys. Res.*, **89**, 9475–9503.